# METAL – POLYMER COMPOSITE NANOFIBER PRODUCTION BY ELECTROSPINNING

A THESIS SUBMITTED TO
THE GRADUATE SCHOOL OF NATURAL AND APPLIED SCIENCES
OF
MIDDLE EAST TECHNICAL UNIVERSITY

BY

NİHAN KARAKOÇ

IN PARTIAL FULFILLMENT OF THE REQUIREMENTS
FOR
THE DEGREE OF MASTER OF SCIENCE
IN
CHEMICAL ENGINEERING

JANUARY 2009

Approval of the thesis:

## METAL – POLYMER COMPOSITE NANOFIBER PRODUCTION BY ELECTROSPINNING

submitted by **NİHAN KARAKOÇ** in partial fulfilment of the requirements for the degree of **Master of Science in Chemical Engineering Department, Middle East Technical University** by,

Prof. Dr. Canan Özgen ______________
Dean, Graduate School of **Natural and Applied Sciences**

Prof. Dr. Gürkan Karakaş ______________
Head of Department, **Chemical Engineering**

Prof. Dr. Güngör Gündüz ______________
Supervisor, **Chemical Engineering Dept., METU**

Prof. Dr. Üner Çolak ______________
Co-supervisor, **Nuclear Energy Engineering Dept., HU**

**Examining Committee Members:**

Assoc. Prof. Dr. Naime Aslı Sezgi ______________
Chemical Engineering Department, METU

Prof. Dr. Güngör Gündüz ______________
Chemical Engineering Department, METU

Assoc. Prof. Dr. Halil Kalipçilar ______________
Chemical Engineering Department, METU

Assoc. Prof. Dr. Göknur Bayram ______________
Chemical Engineering Department, METU

Dr. H. Emrah Ünalan ______________
Metallurgical and Materials Engineering Department, METU

**Date:** **28.01.2009**

**I hereby declare that all information in this document has been obtained and presented in accordance with academic rules and ethical conduct. I also declare that, as required by these rules and conduct, I have fully cited and referenced all material and results that are not original to this work.**

Name, Last name: Nihan Karakoç

Signature :

# ABSTRACT

## METAL – POLYMER COMPOSITE NANOFIBER PRODUCTION BY ELECTROSPINNING

Karakoç, Nihan
M.Sc., Department of Chemical Engineering
Supervisor: Prof. Dr. Güngör Gündüz
Co-supervisor: Prof. Dr. Üner Çolak

January 2009, 95 pages

This study aims synthesis of metal/polymer one dimensional nanostructures by micelle formation, reduction, and electrospinning route, and to analyze the morphological characteristics of composite nanofibers. The study was carried out in three main steps. First, the reverse micelle structures were established between the anionic surfactant and the metal ion. The surfactant acts as an agent to bind metal ions together so that the arrangements of metal ions can be controlled in the solution. As the surfactant concentration increases, reverse micelles grow and reverse wormlike micelle structures are observed. Wormlike micelles are elongated semi flexible aggregates which form a spherocylinder form repeating units. Metal ions are in the core and surrounded with the surfactant. The polymer attached to the wormlike structure acts as a shield and prevents phase separation in a hydrophilic medium. Different polymer and surfactant concentrations were tried to determine the optimum polymer and surfactant concentrations for reverse micelle formation. The size analyses of the reverse micelle structures were done by dynamic light scattering technique. In the second step, metal ions in the micelles were reduced by using hydrazine hydrate to obtain metal cores in the center of wormlike micelles. Finally, electrospinning was carried at room temperature and in air atmosphere. The characterization of nano composites was done by Scanning Electron Microscopy.

It was found that the size of the reverse micelle structures affects the distribution of metal nano partices in polymer nano fibers. In order to distribute the metal nano particles homogeneously, the optimum size of reverse wormlike micelles was found to be between 420 and 450 nm.

**Keywords:** Metal/Polymer Nanocomposite, Electrospinning, Organometallic, Wormlike Micelle, Hydrazine Hydrate.

# ÖZ

## ELEKTRO EĞİRME (ELECTROSPINNING) YÖNTEMİ İLE METAL/POLİMER KOMPOZİT NANOFİBER ÜRETİMİ

Karakoç, Nihan
Yüksek Lisans, Kimya Mühendisliği Bölümü
Tez Yöneticisi: Prof. Dr. Güngör Gündüz
Ortak Tez Yöneticisi: Prof. Dr. Üner Çolak

Ocak 2009, 95 sayfa

Bu çalışmada anyonik yüzey aktif madde ile metal iyonlarının etkileşiminden oluşan kurtçuk misel yapıları kullanılarak metal polimer kompozit nanofiber üretimi amaçlanmıştır. Kompozit nanofiber üretimi temel olarak üç aşamada gerçekleştirilmiştir. Önce metal iyonu ve anyonik yüzey aktif madde arasında ters misel yapılarının oluşumu sağlanmıştır. Yüzey aktif madde metal iyonlarını kendisine çekerek, iyonların çözelti içerisinde denetimli olarak dağıtılmasına olanak sağlamaktadır. Çözelti içerisindeki yüzey aktif madde derişimi arttıkça, oluşan ters misel yapıları büyümekte ve ters kurtçuk misel yapıları oluşmaktadır. Ters kurtçuk misel yapılarının merkezinde metal iyonları bulunmaktadır. Çözeltiye eklenen polimerin hidroksil gruplarının yüzey aktif maddelerin kuyrukları ile oluşturduğu etkileşim sayesinde polimer zincirleri kurtçuk misel yapılarını çevrelemektedir. Hidrofilik bir çözücüde faz ayrımı bu çevreleme ile önlenmiştir. Kurtçuk misel oluşumunda uygun molar oranlarını bulmak için, farklı miktarlarda polimer ve yüzey aktif madde içeren çözeltiler hazırlanmış ve bu çözeltilerdeki misel yapılarının boyut analizi dinamik ışın saçılımı tekniği ile yapılmıştır. İkinci aşamada, ters kurtçuk misellerin merkezinde bulunan metal iyonları hidrazin hidrat ile indirgenerek metal nano parçacıkları elde edilmiştir. Son olarak çözeltinin elektroeğrilmesi ile metal-polimer kompozit nanofiberler üretilmiştir. Üretilen nanofiberlerin morfolojik analizleri taramalı elektron mikroskop kullanılarak yapılmıştır.

Yapılan çalışmada, ters kurtçuk misel yapılarının boyutundaki değişmelerin metal nano parçacıkların polimer nanofiberleri içerisindeki dağılımına olan etkisi incelenmiştir. Ters kurtçuk misel yapılarının boyutları 420 ile 450 nm arasında olduğunda, metal nano parçacıkları polimer nanoliflerin içerisinde düzgün olarak dağılmaktadır.

**Anahtar sözcükler:** Metal/Polimer Nanokompozit, Elektroeğirme,
Organometalik, Kurtçuk Misel, Hidrazin Hidrat.

To Nebi and Hicran Karakoç

&

In the Memory of My Beloved Grandmother Nemide Özmert

# ACKNOWLEDGEMENTS

First and foremost, I would like to express my sincerest gratitude to Prof. Dr. Güngör Gündüz for his magnificent supervision, endless patience, politeness, friendship and invaluable humanity. As my supervisor; he guided me not only on my thesis but also on my life to make me a better, knowledgeable, and stronger person.

I would like to thank to my co-supervisor Prof. Dr. Üner Çolak for helping me with his great ideas and valuable guidance. I am grateful to Assoc. Prof. Dr. Bora Maviş for his endless supports and motivating conversations.

Financial supports of The Scientific and Technological Research Council of Turkey (TUBITAK) and METU–BAP are also acknowledged.

I am very thankful to my laboratory friends Berker Özerciyes, Ahmet Göktaş, Erkan Biber, Korhan Sezgiker, Burcu Berna Topuz, Simge Çınar, Gülden Eroğlu and Nagehan Keskin for their valuable friendship and help. I would also thank to Seçkin Öztürk and Sedat Canlı from Central Laboratory of METU for helping me on SEM analysis.

I would like to give my special thanks to Hülya Tatas, Özge Deniz Yılmaz and Evrim Akyürek for being my family in Ankara. I also would like to thank to Verda Yarangüme, Didem Özmen, Hatice Ceylan and all other friends that I forgot to name here for their special friendship and endless encouragement.

I would like to thank Tuğba Taner, Filiz Daragenli, Mehmet Ekren and Egemen Bilge for their invaluable friendship and being my support in all

aspects of life. They never let me feel alone from the beginning of our childhood.

I would like to express my most sincere thanks to K. Toygar Özgüneylioğlu for his endless help, toleration, and fantastic support. He believed in me and made me believe in myself. This study would not be complete without him.

Last but not least, I would like to thank my beloved family for every beautiful thing in my life. They made me feel as the most precious person in the world. Whenever I feel exhausted, they are my support to get back on my feet, and feel stronger. What I know about beauty, courage, humanity, and goodness is that I learned from them.

# TABLE OF CONTENTS

CHAPTERS

APPENDICES

# LIST OF FIGURES

**FIGURES**

# LIST OF TABLES

TABLES

# NOMENCLATURE

| | |
|---|---|
| C | Concentration |
| CMC | Critical Micelle Concentration |
| cp | Centipoise |
| DC | Direct Current |
| g | Gram |
| h | hour |
| $K_b$ | Dissociation Constant |
| kV | Kilovolt |
| m | Meter |
| M | Molarity |
| ml | Mililiter |
| mm | Milimeter |
| $M_w$ | Molecular Weight |
| MΩ | Megaohm |
| µl | Microliter |
| µm | Micrometer |
| n | Mole |
| nm | Nanometer |
| R | Composition |
| V | Volt |
| w | Weight |
| $^0$ | Degree |
| $^0C$ | Celsius Degree |

# CHAPTER 1

# INTRODUCTION

There is a considerable interest on the synthesis of one-dimensional (1–D) nanostructures such as nanofibers, nanotubes and nanowires due to their desirable functionality and performance. There are many studies aiming the formation of polymer and ceramic based 1-D structures. However, studies on 1-D nanostructures containing metallic entities are less common, but they are expected to provide unique functionalities. The purpose of the current study is to synthesize metal/polymer 1-D nanostructures by micelle formation, reduction, and electrospinning route and analyze the morphological characteristics of composite nanofibers.

Generally, fibers with diameters below 500 nm are referred to nanofibers. Compared with their bulk microstructures form, they have extremely high surface to weight ratio which supplies them flexibility and high directional strength[1]. Due to these characteristics, they are preferred in many applications; especially in medical and filtration[2, 3]. Tissues of human organs could be imitated efficiently in nanofiber form. Also for the filtration applications, nanosized fibers have low air resistance and high efficiency due to the nanopores. Personal care, insulation, energy storage, garments and composite applications are the developing usage areas of nanofibers. The general morphologies of nanofibers are shown in Figure 1.1.

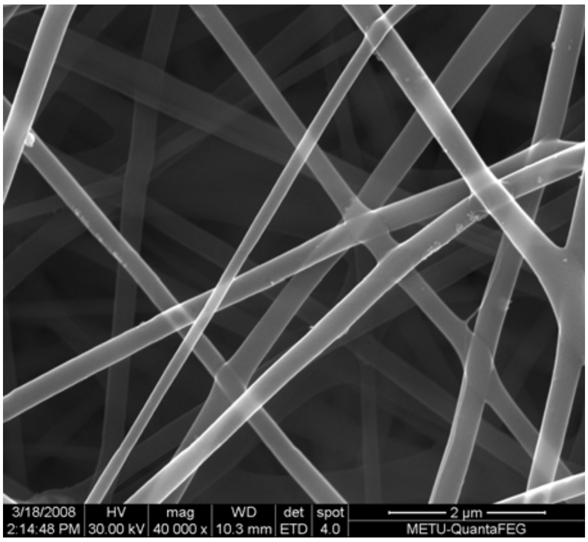

**Figure 1.1** SEM micrograph of nanofibers.

Nowadays, polymeric and ceramic nanofibers can be produced by simple methods and their composite applications are very widely investigated in laboratory scaled experiments. Several studies were done to modify nanofibers in terms of tensile strength, mechanical and chemical resistance. Application fields of nanofibers by considering the data of US patents[2] are presented in Figure 1.2.

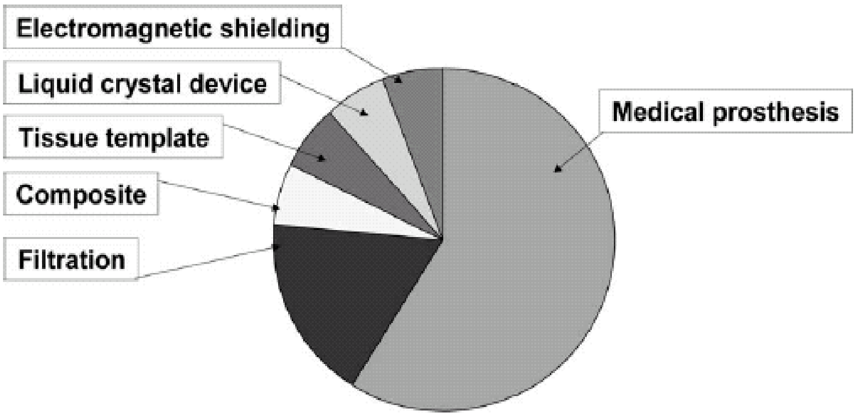

**Figure 1.2** Application fields targeted by US patents.

Also conductive properties of polymers were modified by producing metal - polymer nano composite structures, which also could be used as interconnects in electronic and sensing devices. Various metals; Titanium (Ti)[4], Silver (Ag)[5-7], Nickel (Ni)[8], Copper (Cu)[9], Cadmium (Cd)[10], and Gold (Au)[11] were used to form the composite structure. Transition metals are preferred due to their unpaired outer shell electrons, which supplies them higher interaction with ions when compared with other metals. In literature, mainly hydrophilic or amine group containing polymers are preferred to build the composite structure. Amine groups in the polymer increase the interaction between the metal and the polymer. When hydrophilic polymers are preferred, surfactants (surface active agents) can be used to increase the interaction between the metal and the polymer[12-15].

Among these successful studies, the effects of micellization on composite nanofiber morphology were not investigated. Also, the effect of polymer and surfactant concentration on reversed wormlike micelle formation was not investigated in literature. The distribution of metal ions in the solution was controlled by placing the metal ion in the center of the reverse micelle structure. The effect of shielding polymer in a hydrophilic medium was also firstly introduced to the literature. The relation of reverse wormlike micelle size on the composite nanofiber morphology was also investigated in details.

In this work, aim is the production and characterization of nanocomposite structures from organometallic compounds composed of hydrophilic polymers and transition metals by electrospinning.

The study is carried out in three main steps. First, the micelle structure is established between the anionic surfactant and the metal ion. The surfactant acts as an agent to bind metal ions together. Micelles grow above the critical micelle concentration of the surfactant and wormlike micelles are observed. When ionic surfactants are preferred, in case the presence of a counter ion the reversed micelle structures will grow. The alignment of counter ions in the solution can be achieved by encapsulating them in the reversed micelle structures. Especially, nanorod and nanowire structures are built by establishing the reverse micelle structure between the metal ions and surfactants[10, 16]. By taking the advantage of surfactants on regulating metal ions in the reverse micelle structure, the structure was built by using surfactant molecules and metal ions.

PVA (polyvinylalcohol) and DSS (dioctylsulfosuccinate sodium) were used as the polymer and surfactant, respectively. Copper(II)chloride was used to investigate the parameters affecting the formation of Cu-PVA nano composite nanofibers.

The effects of the concentrations of polymer and surfactant on wormlike micelle formation were investigated. The optimum amounts of surfactant and polymer were determined by using a wide angle particle size analyzer. It was found out that average particle size was increasing with the increase of the concentrations of surfactant. The concentration limits of the polymer and surfactant were determined in order to have a homogeneous solution.

The reversed micelle structure was shielded by a hydrophilic polymer, which prevents phase separation in a hydrophilic solvent. The shielding polymer also kept the reverse micelle structure together after the reduction of metal ions.

In the second step, metal ions in the micelles were reduced obtain wormlike micelles with metal cores. Various reduction agents can be employed to reduce metal ions in the solution. The efficiency of the reduction reaction is proportional to the active groups of the reducing agents. Most common reduction agents are hydrazine hydrate[5, 9, 10, 17-19], sodium azide[7, 19], dimethylformamide[19], and sodium formaldehyde sulfoxylate[6]. Among these reduction agents hydrazine hydrate has the most efficiency on reducing the transition metals[6, 19]. Metal ions were reduced to metal nanoparticles by hydrazine and the optimum reaction concentrations were found experimentally.

Finally, electrospinning of the solution is carried out and optimum electrospinning parameters were identified to obtain defect free and continuous nanofibers composed of Cu-PVA. Nanofibers were characterized by SEM.

# CHAPTER 2

# LITERATURE REVIEW

The selected route for the synthesis of 1-D metal/polymer composite was based on the building of the composite structure using surfactants to obtain reversed wormlike micelle formation, encapsulation of metallic ions within the micelle structure, and shielding the micelle by hydrophilic polymer.

Once this structure is obtained, it was expected to reduce metal ions to metallic form by an appropriate reducing agent. Finally, the formation of 1-D composite structure was carried out by creating nanofibers using electric field forces for stretching the polar solution.

In this chapter, the previous studies in literature were reviewed. The surface active agents, their types and micellization behavior are presented in Section 2.1. Also the dynamics of micelle and reverse micelle formation was presented in this section. Wormlike micelle structures and their characteristics are given in Section 2.2. by introducing previous works in literature. The studies about the size control of nano emulsions by means of surfactants are also illustrated in this section. Size analysis techniques of micelle structures and reduction routes of metal ions are discussed in Sections 2.3 and 2.4. Electrospinnig technique and parameters affecting on product quality are introduced in Section 2.5, while previous studies about electrospinning of PVA were given in Section 2.6. Previous studies about metal polymer nano composite structures are given in Section 2.7.

## 2.1 Surface Active Agents

Surfactants are organic compounds and generally have both the hydrophilic and hydrophobic groups, which make them soluble in large variety of solvents. They can reduce the surface tension and the free energy of the solvent molecules because they are adsorbed at the liquid gas interface for one phase solutions. They also adsorbed in liquid – liquid interface for the solutions containing two immiscible liquid and ease the dissociation in the solution[15]. Due to these characteristics, surfactants have various application areas such as; oil recovery from water, detergency and development of drug delivery. A representative figure for the surfactant molecule is given in Figure 2.1.

**Figure 2.1** A representative figure for the surfactant molecule.

The hydrophilic head of the surfactant can be anionic, cationic, zwitterionic, and nonionic, which identifies the ionic behavior of the surfactant molecule[20].

In the solution, the concentration (C) of surfactant molecules controls the interaction of them with other surfactant molecules. For the dilute solutions, the interactions of the surfactant molecules are very weak. With the increasing surfactant concentration, stronger interactions are observed. There is an important value of concentration called as critical micelle concentration (CMC)[16]. Below CMC, the interaction of the tails is not sufficiently high to establish the micelle structure. The surfactant molecules in the solution are shown schematically in Figure 2.2.

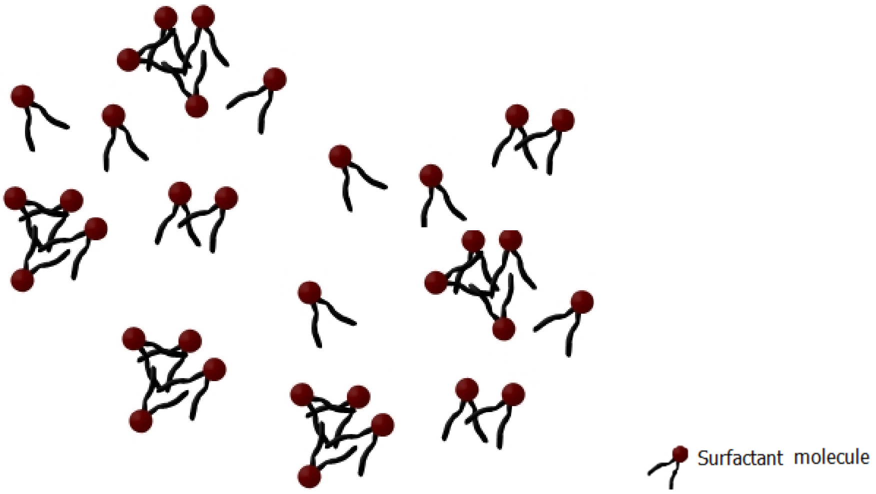

**Figure 2.2** Surfactant molecules in the solution when C<CMC.

Above CMC, surfactant molecules can form micelle structures, which are nano emulsions in the solutions. The hydrophobic groups of the surfactant molecules are directed inside the micelle, which decreases the free energy of the solution considerably. The main idea behind the micelle formation is minimizing the free energy in the system. Surfactant are aggregated so that the hydrophobic groups directed to the center of clusters and hydrophilic groups are directed toward the solvent molecules. Hydrophobic groups are partly removed from the contact with solvent molecues and free energy of the system was reduced[15].

The interactions between the hydrophobic tails of the surfactants keep the micelle structures together. A schematic representation of a micelle formation was given in Figure 2.3.

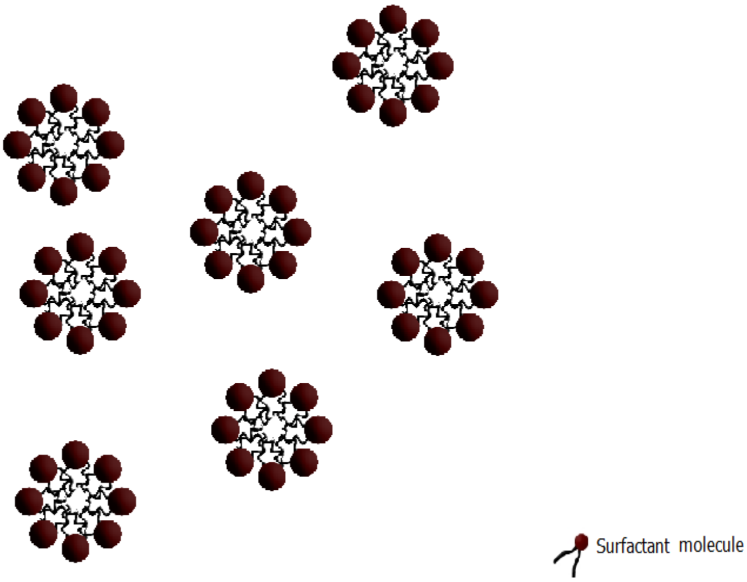

**Figure 2.3** Micelle structure formed by surfactant molecules.

When the surfactant concentration is further increased, the micelle structures will grow. The shape of the growth is determined by the hydrophobic tail of the surfactant molecules.

The entanglements of hydrophobic tails keep the micelle structure together. Solution temperature, pH, presence of organic compounds, the binding of a counter ion, type of the surfactant and the ionic strength of the surfactant affect the micelle formation characteristics of the surfactant. The hydrophobic tail of the surfactants can have a various groups; common groups were given in Rosen, 2004[15]:

- Straight chain, long alkyl groups,
- Long chain alkylbenzene residues,
- Alkylnaphthalene residues,

- Rosin derivatives,
- High molecular weight propylene oxide polymers,
- Long chain perfuoroalkyl groups,
- Polysiloxane groups.

Increasing surfactant concentration, micelles interact with each other and grow. The tail groups of the surfactant molecules also affect the growth behavior of the micelles. Depending on the tail groups, surfactants can be classified into three main groups[21]; single chain, gemini and trimetric. The schematic representation of surfactant types were given in Figure 2.4.

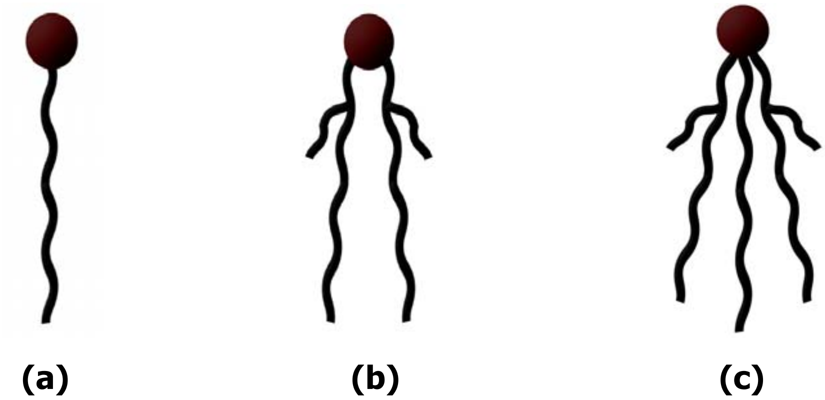

**Figure 2.4** A representative figure for the surfactant types; **(a)** single chain, **(b)** gemini, **(c)** trimetric.

The shape of growth is dependent on the type of the surfactant. The interaction strength of the tails determines the shape of the growing wormlike micelle structures. Wu et al. modeled the growth of the micelles in their study. Figure 2.5 represents the models by Wu et al.[21]

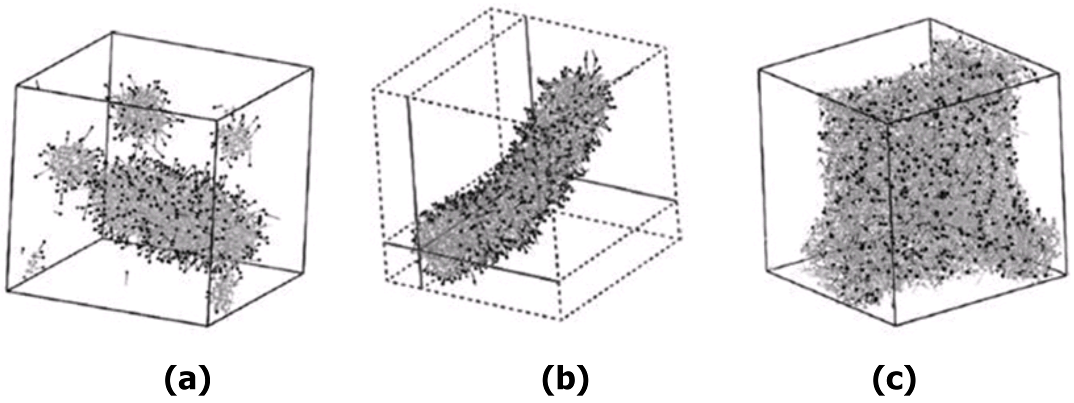

**Figure 2.5** Growth of the micelles. **(a)** Single chain, **(b)** Gemini, **(c)** Trimetric. [21]

The growth of micelles composed of single chain surfactants is small and spherical while it is elongated cylindrical rodlike and large lamellar for the micelles composed of gemini and trimetric surfactants respectively.

For the ionic surfactants, in the presence of a counter ion in the solution, reversed micelle structures are formed due to the binding effect of the counter ion. The ionic heads of the surfactants direct toward the counter ion and the tails are directed outside. Also for the reverse micelle structure, the interactions of hydrophilic tails keep the surfactant molecules together in the micelle.

The surfactant concentration is very low, micelle structures could not be formed completely as shown in Figure 2.6. Only a few of the surfactant molecules surround the oppositely charged ion. The interaction that leads the micelle formation cannot be established between the surfactant molecules because the number of molecules in the solution is not sufficient.

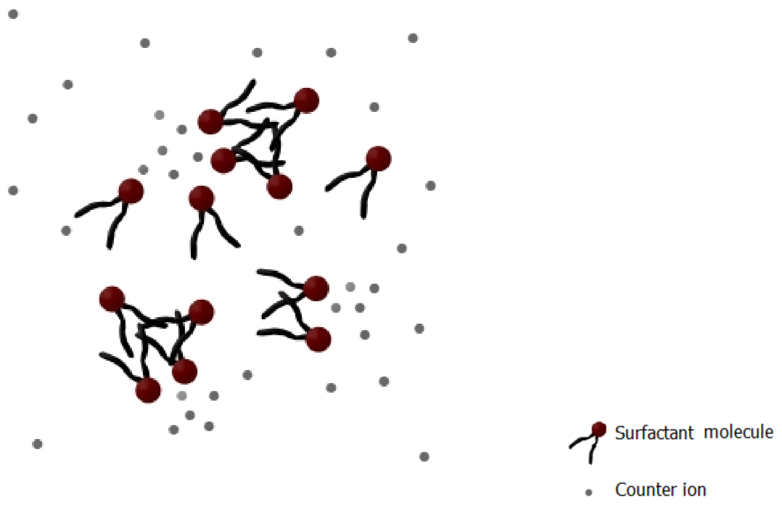

**Figure 2.6** Surfactant molecules and counter ions in the solution when C<CMC.

Increasing surfactant concentration increases the interaction strength of the hydrophobic tails of the surfactant molecules. Surfactant molecules are directed to the counter ions due to ionic interaction and the structure is kept together due to the interaction of the hydrophobic tails. The counter ions are encapsulated in the reversed micelle structure.

The alignment of counter ions in the solution can be achieved by encapsulating them in the reversed micelle structures. Especially, nanorod and nanowire structures are built by establishing the reverse micelle structure between the metal ions and surfactants[10, 16].

The metal ions in the solution can be reduced after the micelle structure is established and metal nanorod and nanowire structures are observed. The schematic representation of reversed micelle structure is illustrated in Figure 2.7.

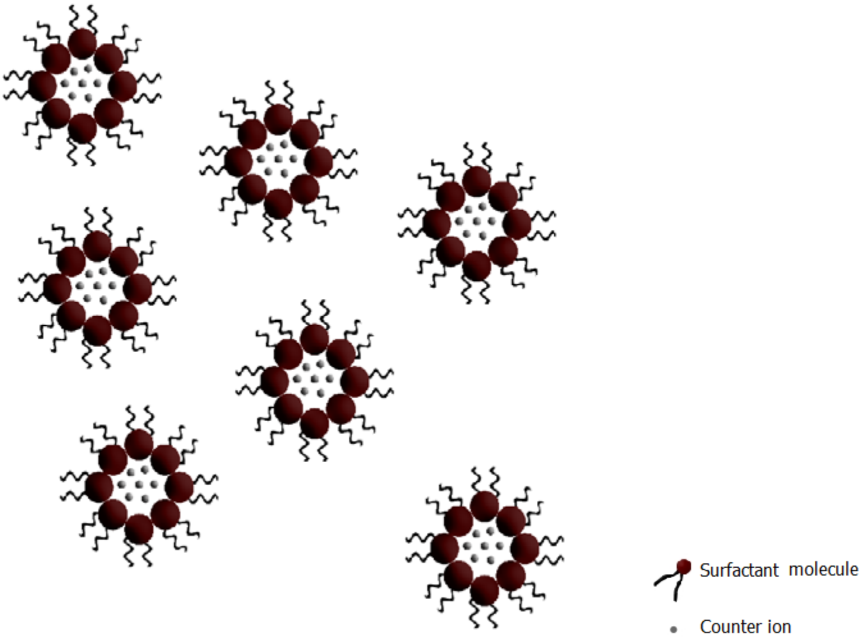

**Figure 2.7** Reversed micelle structure.

As shown in Figure 2.7, counter ions (illustrated as gray points) attracts the ionic head of the surfactant molecules and micelle shape is reversed. Due to this characteristic of surfactant molecules, ionic molecules can be ordered in the solution by attaching at the center of micelles[20]. This reverse orientation the free energy of the system is increased because the hydrophobic groups of the surfactants are directed toward the solvent molecules. Phase separation may occur in a hydrophilic solvent unless the hydrophobic groups of the surfactant molecules are shielded with a hydrophilic polymer[15, 21]. The shielding effect of hydrophilic polymers can balance the free energy of the system. They can interact with the hydrophobic part of the surfactant molecules and surround the structure, the solvent molecules will not interact with the hydrophobic part of surfactant molecules. The schematic representation of the reversed micelle structure surrounded by a hydrophilic polymer is given in Figure 2.8.

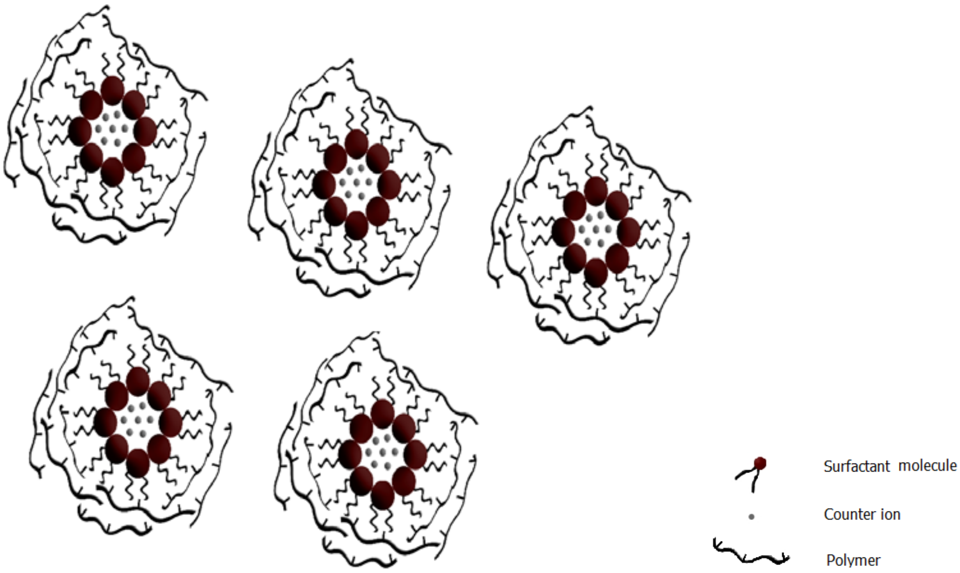

**Figure 2.8** Reversed micelle structure surrounded by a hydrophilic polymer.

The size of the reversed micelles also depends on the hydration radius of the metal ion. All metal and non metal molecules are surrounded by water molecules when dissolved in water. They interact with the nearby water molecules because of the attraction of unpaired electrons in oxygen. This layer of water molecules is called as hydration sphere[22]. The schematic representation of a hydrated metal ion given by Wulfsberg is illustrated in Figure 2.9.

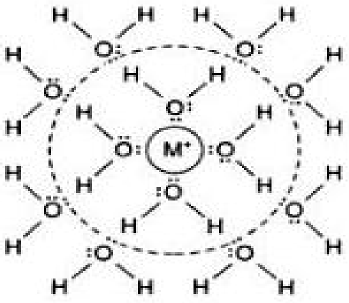

**Figure 2.9** Hydration radius of a metal ion.[22]

The hydration radius of a metal ion depends on both the molecular weight and the charge of the ion. For the ions with the same charge, radius of hydration is proportional to the molecular weight of the metal, because the number of outer shell electrons depends on the molecular weight of the metals[23].

Some of the water molecules in the radii of hydration are replaced by surfactant molecules, when anionic surfactant molecules are added to a solution containing metal ions. This replacement is forced by the ionic interaction between the metal ion and anionic head of the surfactant. The formation of the reversed micelle structure is shown in Figure 2.10.

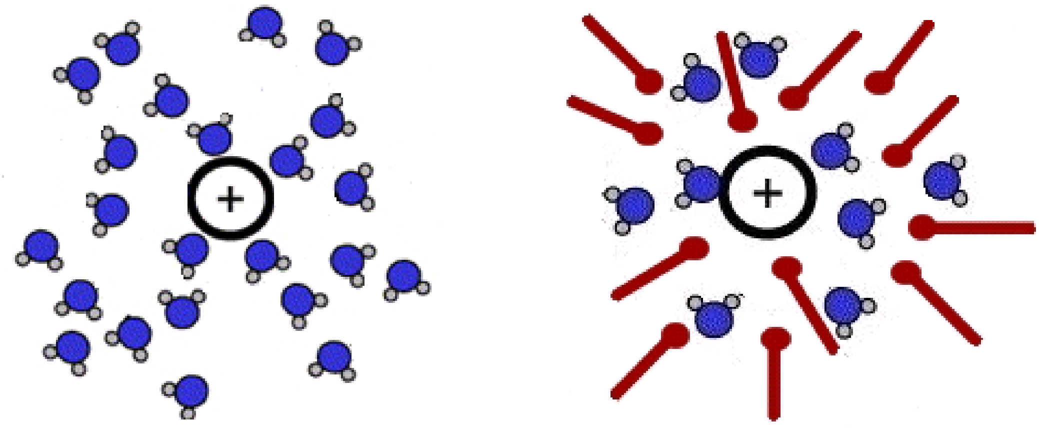

**(a)** **(b)**

**Figure 2.10** Hydration radius of a metal ion **(a)** without the presence of surfactant molecules[23], **(b)** reversed micelle formation.

## 2.2 Wormlike Micelles

Wormlike micelles are elongated semi flexible aggregates formed by gemini type surfactants. Hait et al[24] investigated the gemini type surfactants and reported most common gemini type surfactants that lead to wormlike micelle structure.

- Pinacyanol chloride,
- Decyl sulfate sodium,
- Dodecyl-trimethylammonium bromide,
- Dodecyl sulfate sodium,
- Dioctyl-sulfosuccinate sodium,
- Tetradecyl-trimethylammonium bromide,
- Cetyl-trimethylammonium bromide,
- Dodecyl-benzenesulfonate sodium.

are the most common surfactants reported on the studies about gemini type surfactants[14, 24].

Gemini type surfactants can pack very close with each other. Their branched alkyl chains provide excellent wetting properties. Short linkage geminis (C~12) can form wormlike micelles (see Figure 2.4 - b), which also have unique adsorption properties on oppositely charged surfaces[15]. Repeating units form a spherocylinder, in which bonds are broken and combined continuously. The solution viscosity is considerably increased due to the entanglements of wormlike micelle structures. The schematic representation of wormlike micelle structure is shown in Figure 2.11.

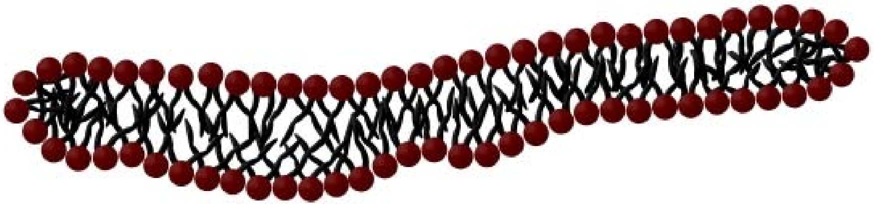

**Figure 2.11** Wormlike micelle structure.

This study is mainly concerned on the reverse wormlike micelles formed with metal ions and gemini type surfactant molecules. The presence of metal ions leads the reverse wormlike micelle formation and the interaction of surfactant molecules keeps the structure together. Metal ions are encapsulated in the wormlike micelle structure and distribution of metal ions in the solution can be controlled with the built reverse wormlike micelle structure. The schematic representation of reversed wormlike micelle structure is given in Figure 2.12.

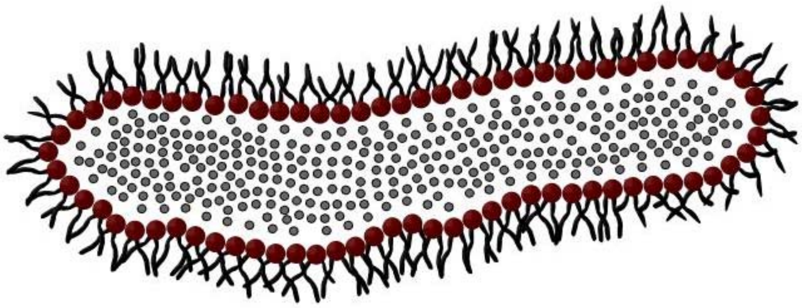

**Figure 2.12** Reversed wormlike micelle structure.

Hait et al[24] investigated the synthesis route and main characteristics of dioctyl-sulfosuccinate sodium (DSS). It was reported that, CMC was remarkably low when compared with other surfactants. It can form micelle structures at lower concentrations when compared with conventional surfactants. The anionic part lowers the CMC and makes less sensitive to the polarity of the solvent by increasing the stability of micelle structures.

DSS can form reverse micelles if the solvent is very polar or there is a counter ion in the solution. The cations or polar groups interact with the anionic head of the surfactant and head groups of DSS are directed to the counter ion and the surfactant molecules surrounds the counter ion by forming reversed micelle structure[25]. The CMC of DSS was reported as $6.4\times10^{-4}$ M[26].

Feader et al[25] simulated the reverse micelle structure of DSS in water – isooctane system with excess addition of Sodium ($Na^+$) ions to the solution. It was found that the ratio of DSS to water and $Na^+$ ions determined the shape and stability of reversed micelle structures. The presence of isooctane prevented the precipitation of reversed micelles. The hydrophilic tails of DSS were directed outside and they would cause phase separation if isooctane would not be in the system.

Charlton et al[20] investigated the formation of the reverse micelle structure between DSS and ferricyanide ($Fe(CN)_6^{3-}$) by using phase transfer technique with a supporting electrolyte in water – isooctane system. It was determined that encapsulating of counter ions with reversed micelle structure could build the micro electrolytes. The efficiency of the micro electrolytes was found to be dependent on the established reverse micelle structure, which was controlled by adjusting the molar ratios of ferricyanide and DSS. Cringus et al[27] investigated the formation reverse micelle structure formation in water – DSS and n-octane system. It was stated that, by confining water in one or more spatial dimensions, nanoscale water cavities and interfacial hydrophobic interactions can be neutralized. With this method, nano sized water droplets were covered with a monolayer of DSS molecules and miscibility of two immiscible liquids was achieved. By this approach the polar solvent molecules could be made miscible in non polar solvents. By using the advantage of formed reverse micelle structures, fast dephasing dynamics could be slowed and mobility of the interfacial water could be investigated. Besides these advantages, reverse micelle structures are also efficient in size and shape control of nanostructures.

Xi et al.[10] constructed the reverse wormlike micelle structure between Cadmium (Cd) and DSS. It was found that the nucleation and growth of Cd nanoparticles are dependent on the DSS concentration. Nanorods were observed from spherical Cd nanoparticles with the increasing concentration of DSS.

By considering the previous studies, in this thesis, the model for Cu – DSS reverse micelle structure was built. The effect of changing DSS concentration was investigated. The selection of molar ratios was done by considering the previous works and the thermodynamic radius of ions.

## 2.3 Dynamic Light Scattering

Dynamic light scattering (DLS) is a useful method to measure average particle size of clusters in the solution. The aggregation numbers of wormlike micelles are directly proportional to the surfactant concentration[28]. The characterization of wormlike micelle structures with respect to the changing surfactant concentration can be done by using DLS analysis. The main idea of analyzing suspended particles is to measure the motion of the particles in the solution. This motion is called as Brownian motion. Brownian motion describes the random movement of particles in a solution. In DLS, the diffusion speed of the moving particles can be measured. The measurements were done in Polystyrene cells.

Size measurements can be done either with a constant $90^0$ detector or a wide angle moving detector depending on the solution characteristics. For the solutions having low solute concentration (below 0.1%), constant detector can be used. When the solute concentration is increased above 5%, wide angle moving detectors are preferred[28]. In a $90^0$ system the laser passes through the center of the cell and the scattering is observed at $90^0$, which means laser beam should travel to the center of the cell. In case of concentrated solutions, the laser beam will come across with many suspended molecules. This effect of suspending particles is called as multiple scattering effects. This causes loss of intensity, which would lead to inaccurate measurements. In wide angle analysis, the measurement points can be varied and the laser travels a shorter distance in the cell, so multiple scattering effects can be minimized. Especially, the wormlike micelle structures increases the viscosity of the solution. Therefore wide angle scattering is preferred for the size measurements of the samples.

## 2.4 Reduction of Metal Ions in Solution

Various reduction agents can be employed to reduce metal ions in the solution. The efficiency of the reduction reaction is proportional to the active groups of the reducing agents. Most common reduction agents are hydrazine hydrate[5, 9, 10, 17-19], sodium azide[7, 19], dimethylformamide[19], and sodium formaldehyde sulfoxylate[6]. Among these reduction agents, hydrazine hydrate has the most efficiency on reducing the transition metals[6, 19].

The amino (–$NH_2$) groups of hydrazine hydrate are very reactive and interact with the outer shell electrons of metals easily. Besides, reduction reaction of hydrazine hydrate does not have residual side products.

In the studies, where hydrazine hydrate was used as reducing agent, hydrazine hydrate was dissolved in the water. $N_2H_5^+$ ions, which initiate the reduction reactions, were observed as the product of the dissociation of hydrazine hydrate. The dissociation of hydrazine hydrate was investigated by Li et al[29] and observed dissociation reactions are given in Equations 2.1 and 2.2 with their $K_b$ values.

$$N_2H_4 + H_2O \rightarrow N_2H_5^+ + OH^- \qquad K_b = 3\times10^{-6} \qquad (2.1)$$

$$N_2H_5^+ + H_2O \rightarrow N_2H_6^{2+} + OH^- \qquad K_b = 8,4 \times10^{-16} \qquad (2.2)$$

The mechanism given in Equation 2.2 is not favored and $N_2H_5^+$ is assumed to be the only product in the dissociation reaction of hydrazine hydrate.

The efficiency of reduction agents was compared in several studies. Ghosh et al.[19] investigated the reduction efficiency of sodium azide and hydrazine hydrate on reducing silver ions. Silver nitrate ($AgNO_3$) was used as silver ion supplier. Dimethyl formamide (DMF) was used as solvent for the reaction of sodium azide, while ethanol – water mixture was used for the reaction of hydrazine hydrate. Pure silver nanoparticles were not observed for the reactions carried with sodium azide. Silver azide particles were synthesized.

Pure silver nanoparticles were observed by using hydrazine hydrate as the reducing agent. The reaction kinetics were also investigated predicted reaction mechanism was given in Equation 2.3.

$$N_2H_4.H_2O\ (aq) + AgNO_3\ (aq) \rightarrow N_2\ (gas) + 4Ag\ (solid) + H_2O\ (aq) \qquad (2.3)$$

When the molar ratio of silver ions to hydrazine hydrate is 1:2.5, reduction reaction is completed with 99.15% efficiency resulting in submicron silver particles at room temperature.

Xi et al[10], produced Cadmium Selenide (CdSe) nanorods by using hydrazine hydrate both as reducing and templating agent. Cadmium Nitrate ($Cd(NO_3)_2$) and Sodium Selenite ($Na_2SeO_3$) was used to synthesize CdSe. It has been found when the molar ratio of cadmium of hydrazine hydrate was 7.8 maximum rod size was achieved. If amount of hydrazine hydrate was further increased, the nanorod structure was destructed due to the bridging effect of hydrazine hydrate. Excess hydrazine hydrate amount caused the coagulation of CdSe nano particles and spherical aggregates were observed.

Li et al[29], synthesized Zinc Telluride (ZnTe) nanorod structures by using hydrazine hydrate both as reducing and electron transfer agent. It was investigated the formation of nanorod morphology and concluded that the bridging effect of hydrazine hydrate eases the nanorod formation and size of the nanorods could be controlled by changing molar ratio of hydrazine hydrate in the solution.

Demir et al[30] synthesized polyacrylonitrile (PAN) nanofibers and hydrazine hydrate was used for surface treatments of synthesized fibers. The fiber mats were immersed into a dilute hydrazine hydrate solution and $-NH_2$

groups of hydrazine hydrate was attached to the surfaces of nanofibers. By introducing fiber mats into silver nitrate solution, silver nanoparticles were attached to the fiber surface. The silver ions were reduced at the surface of nanofibers. The reducing and binding effect of hydrazine hydrate was used to bind the silver nano particles on polymer surfaces.

Songping[8] synthesized nickel copper nano particles by reducing nickel ions and copper oxide with hydrazine hydrate. It was found that the shape control of nanoparticles can be achieved by the control of the hydrazine to metal ion ratio. The proposed reaction mechanisms were given in Equations 2.4 and 2.5 for copper oxide and nickel respectively.

$$N_2H_4.H_2O + CuO \rightarrow N_2 + H_2 + 2Cu + 2H_2O \tag{2.4}$$

$$N_2H_4.H_2O + 2Ni(OH)_2 \rightarrow N_2 + 2Ni + 5H_2O \tag{2.5}$$

Wang et al[16] worked on surfactant assisted morphology control and synthesis of cube shaped lead telluride (PbTe) and lead selenide (PbSe) nanorod structures. A hydrothermal process was used in the presence of polyvinyl pyrolidone (PVP). Nanorods with uniform size were synthesized. The predicted reduction mechanism for the reduction reaction was given in Equation 2.6.

$$2Pb^{2+} + N_2H_4 + 4OH^- \rightarrow 2Pb + N_2 + 4H_2O \tag{2.6}$$

The proposed reaction mechanism was the same in every study, which claims that one mole of hydrazine hydrate can reduce four moles of +1 charged ion. It was found that to carry the reaction to completion, excess amount of hydrazine hydrate was needed[5, 9, 10, 17-19]. The molar ratio of excess hydrazine hydrate was determined by considering the solution characteristic in each study.

## 2.5 Electrospinning of the Solution

Nanofibers can be produced by several methods, namely phase separation[31,32], self assembly[33, 34], drawing[35, 36], and electrospinning[1, 2, 37-39]. Among these processes, phase separation can only be applied for specific polymers. Though very small fiber diameters can be observed in self assembly process, controlling fiber size in self assembly process is not easy due to high number of variables. Drawing is a very simple technique to obtain nanofibers, but continuous nanofibers cannot be produced with controlled fiber diameter. When compared with these techniques, electrospinning is a simple, cost effective process and continuous nanofibers can be produced with controlled fiber diameter.

Formlals[40] patented the idea of producing artificial filaments with electric field force in 1939. The study was about spinning of cellulose acetate fibers, but completely dry filaments could not be obtained. In 1969, Taylor[41] studied the shape of the polymer droplet at the tip of the syringe and he proposed that an angle of $49.3^0$ degree is needed to balance surface tension of the polymer by the applied electric field forces. Number of studies about electrospinning increased tremendously in the 21st century and the interest is continuously developing.

In electrospinning, high voltage is supplied by a DC voltage supplier. The voltage is applied to the solution at the tip of the syringe, where the solution is contained. The flow rate of the solution is regulated with a syringe pump.

The products are collected on a grounded metal collector. Electrospinning is applicable for a wide variety of solutions. Polymeric and ceramic nanofibers can be produced with this technique. Composite applications with organic and inorganic compounds have been investigated in literature[5, 6, 9-11, 42]. A schematic representation of electrospinning process is illustrated in Figure 2.13.

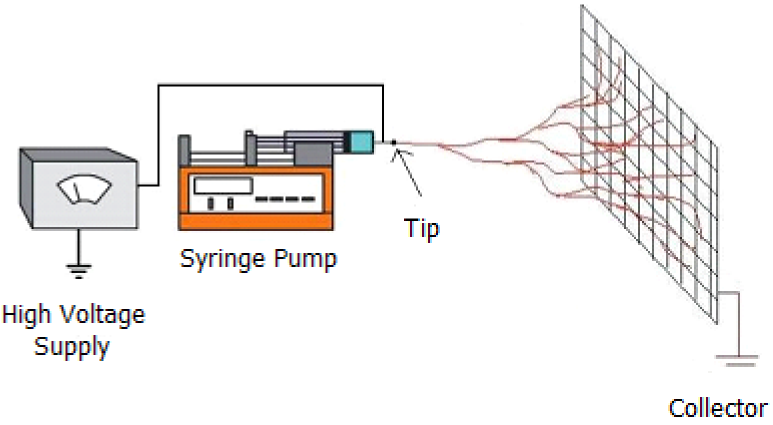

**Figure 2.13** Schematic representation of electrospinning.

Initiated jets are formed at the tip of the syringe, when applied voltage overcomes the surface tension of the fluid. As the syringe pump feeds the solution, the initiated jets are directed along the electric field lines between the syringe tip and the metal collector. During the motion in the air, the solvent evaporates and dry fibers are collected onto the metal collector. Material properties and process parameters are two main parameters affecting the fiber morphology.

Solution viscosity, conductivity, volatility and the surface tension of the solution are the main material properties that affect the quality of the final product. Also by adjusting the feed rate, applied voltage, nozzle collector distance, process temperature and pressure the size of the electrospun fibers can be controlled[1, 33, 43].

## 2.6 Determination of Electrospinning Conditions

Electrospinning of PVA was extensively investigated in previous works[5, 7, 9]. PVA have a large range of application areas such as separation filters, biodegradable mats. PVA is also used as thickening agent for water because the chain entanglements start in low concentration of PVA[44]. Various studies were done to determine proper electrospinning conditions of PVA[45]. The suitable concentration range of PVA was found for electrospinning. Applied voltage can be ranged between 15 and 25 kV by considering the design parameters. The electric forces are balanced by the surface tension of the solution, when the concentration of PVA was between 7% and 12%. In case of the addition of additives such as surfactants or a compatible polymer was added to solution, the percentage of PVA in the solution was decreased below 10% in order to balance the surface tension of the solution with the applied electrostatic forces.

## 2.7 Metal Polymer Nanocomposites

There are several studies in literature, in which polymer metal nano composites were produced by electrospinning technique.

Yang et al[5] prepared PAN nanofibers containing silver nanoparticles. The amine groups of PAN supplied higher interaction with metals when compared with hydrophilic polymers. DMF was used as a solvent in which $AgNO_3$ and

PAN were dissolved. Reduction of silver ions was done by using hydrazine hydrate. No further purification was done to the solution. PAN nanofibers were obtained by electrospinning of the solution. Distribution of Ag nanoparticles was not homogeneous. TEM (transmission electron microscopy) was used to investigate the images of, Ag nanoparticles were found to be on the surface of PAN nanofibers.

Jin et al[46] proposed a way to distribute Ag nanoparticles in polymer matrix to produce antimicrobial separation filters. It was found that polyvinyl pyrollidone (PVP) controlled the formation of silver nanoparticles during the reduction with hydrazine hydrate. It was claimed that the presence of PVP promotes the nucleation of Ag nanoparticles and prevents the aggregation affecting as a shield. Triton X was also used as surfactant to increase the interaction of silver ions with PVP. PVA nanofibers containing silver nano particles were produced by electrospinning technique. By using the solution of $AgNO_3$ and PVP as a precursor, composite nanofibers of PVP and PVA containing silver nanoparticles were prepared. The effect of changing surfactant and polymer composition on distribution of silver nanoparticles in polymer matrix was not discussed in the study.

Kong et al[47] produced PVA and polymethyl methacrylate (PMMA) nano composites containing silver nanoparticles for bio sensing purposes. Methyl methacrylate (MMA) monomers were added to the solution containing PVA and silver ions. As MMA polymerized on the Ag – PVA structures, PMMA coated the structure and keep together during electrospinning. It was stated that changing ratio of PVA affects the morphology of electrospun polymers. It was claimed that PVA acts both as a gelation agent to control the viscosity of the solution and as a protection agent preventing protects silver clusters from sintering.

Hamlett et al[48] produced polyethylene oxide (PEO) nanofibers containing gold nano particles by electrospinning technique. The study investigated the effect of Au and PEO concentration on fiber morphology. The average fiber diameters were decreased with the increasing PEO concentration. The surface tension of the solution was increased and thinner fibers could be produced by electrospinning. When Au concentration was increased, the surface tension of the solution decreased dramatically. Beads were formed on the electrospun fibers. Au nanoparticles were coagulated on the beaded areas. Though Au nanoparticles increased the degree of crystallinity in PEO nanofibers, the distribution of nano particles in polymer matrix could not be controlled with increasing Au concentration.

Li et al[9] built the composite structure between PVA and Cu nanoparticles by electrospinning. DSS was used as surfactant to bind Cu nanoparticles to PVA. Cu nanoparticles were reduced by using hydrazine hydrate. The molar ratio of copper ions to hydrazine hydrate was 1:10. In the study, homogenous distribution of Cu nanoparticles in PVA could not be achieved. Though, Cu nanoparticles were in PVA matrix in some parts of fibers, the distribution was not continuous. The effects of changing surfactant and polymer concentrations on the distribution were not investigated.

Among these successful studies in literature, the effects of surfactant concentration and polymer concentration were not investigated. These effects are vital for the distribution of metal nanoparticles both in the solution and obtained polymer nanofibers.

The key point of distributing metal nanoparticles in solution is encapsulating them in a reversed micelle structure as they were ions. When the ions are encapsulated, their arrangements can be controlled with the size and shape of the micelles. In the presence of a polymer in the solution, micelle structures will be shielded by the polymer and metal particles can be distributed in polymer solution. The reduction of metal ions should be done without destructing the micelle structure. As a result, metal nanoparticles are kept in PVA matrix during electrospinning and distributed homogeneously and continuously in electrospun nanofibers.

The aim of this study was to define the optimum polymer and surfactant concentration to keep the Cu nanoparticles in wormlike micelle structure. The effect of DSS and PVA concentrations on micelle formation was investigated. Cu nanoparticles were reduced by hydrazine hydrate and the optimum reaction concentrations were found by considering previous works in literature.

# CHAPTER 3

# EXPERIMENTAL

This study was performed to obtain 1-D metal/polymer composite structures by direct synthesis using reversed wormlike micelle formation, reduction of metal ions in solution, electrospinning of the polar solution. This methodology was expected to provide an easy one step and cost effective approach to achieve the desired final composite form.

In this chapter, the chemicals used in the experiments are introduced in Section 3.1. while the experimental procedure and characterization techniques are explained in detail in Section 3.2. The experimental procedure is summarized in five main parts; solution preparation, size measurements of reverse wormlike micelles, electric field application to the solution, reduction of metal ions, and electrospinning of the solution.

## 3.1 Materials

### 3.1.1 Polyvinyl Alcohol (PVA)

PVA (Clariant) was selected as the shielding polymer. Its molecular weight was determined at the Central Laboratory of Middle East Technical University by using a Gel Permeation Chromatography (PL-GPC 220). The molecular weight ($M_w$) of PVA was found as 23.000 g/mol. Chemical structure of PVA is shown in Figure 3.1.

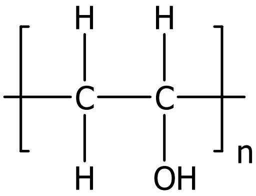

$$\left[\begin{array}{c} \mathrm{H} \\ | \\ -\mathrm{C}- \\ | \\ \mathrm{H} \end{array}\begin{array}{c} \mathrm{H} \\ | \\ \mathrm{C}- \\ | \\ \mathrm{OH} \end{array}\right]_n$$

**Figure 3.1** Chemical structure of PVA.

### 3.1.2 Dioctylsulfosuccinate sodium (DSS)

DSS (Sigma Aldrich, Germany) with 98% purity was used as surfactant to build the reverse wormlike micelle structure. Its molecular weight is 444.56 g/mole. It is a gemini type anionic surfactant and generally used to form wormlike micelle structures. In this study, it was used to form reversed wormlike micelle structure with $Cu^{2+}$ ions. Chemical structure of DSS is given in Figure 3.2.

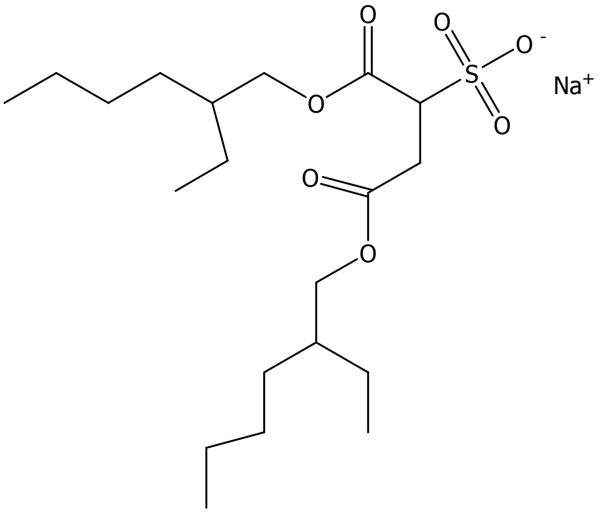

**Figure 3.2** Chemical structure of DSS.

### 3.1.3 Hydrazinium Hydroxide

80% solution of hydrazine hydrate (Merck Darmstadt, Germany) was used to reduce the copper ions. Its molecular weight is 50.0602 g/mole. It is a common reducing agent used to reduce wide variety of metals. The chemical structure of hydrazine hydrate is given in Figure 3.3.

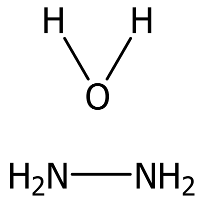

**Figure 3.3** Chemical structure of hydrazinium hydroxide.

### 3.1.4 Other Chemicals

Copper(II)chloride ($CuCl_2$) was used as Cu ion source, and purchased from Merck, KGaA, Germany. Deionized water (DIW, 18.2 MΩ; Human UP 900, Innovation) was used in the preparation of solutions. Sodium hydrogen sulfite ($NaHSO_3$) was purchased from Merck, KGaA, Germany, and used to remove the dissolved oxygen in water. The open chemical structure of $NaHSO_3$ is given in Figure 3.4.

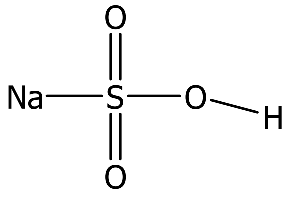

**Figure 3.4** Chemical structure $NaHSO_3$.

## 3.2 Experimental Procedure

### 3.2.1 Solution Preparation

In this study, solutions of PVA, $CuCl_2$, and DSS were prepared by using deionized water as solvent. $NaHSO_3$ was also added to the solution to prevent the oxidation of Cu after reduction. 0.068M $CuCl_2$, 2.4g PVA, and $3.37\times10^{-3}$M DSS was dissolved in 20 ml deionized water.

Homogeneous solution was observed after mixing for 4 h at 50 $^{O}$C. While preparing the solutions, deionized water was further purified by passing through a filter (Millex-HPF LCR Filter Unit, Milipore Corp., USA) with 0.20 $\mu$m pore size to remove any possible impurities. After having homogeneous solutions, the solutions were cooled to 25 $^{0}$C.

In order to investigate the effects of DSS and PVA on wormlike micelle formation, 18 sets of solutions were prepared. Five different DSS concentrations were dissolved in 5 different PVA concentrations. While the amount of DSS was changed, the amount of PVA was kept constant for each set of DSS. The optimum amounts of $NaHSO_3$ and $CuCl_2$ were determined in preliminary experiments and their amounts were kept constant during the size measurements.

The effect of the amount of PVA on solution viscosity was investigated. Viscosity measurements of solutions having different PVA content between 4% and 12% content were made by using a Vibro Viscometer (SV – 10, A&D Company Ltd., JAPAN). The viscosity measurements were done at room temperature under atmospheric pressure. Compositions of all the prepared solutions are tabulated in Table 3.1

**Table 3.1** Solution compositions for particle size analysis.

| $H_2O$ (ml) | $NaHSO_3$ (g) | $CuCl_2$ (g) | PVA (%) | DSS (g) |
|---|---|---|---|---|
| 20 | 0.1 | 0.184 | 4 | 0.001 |
| 20 | 0.1 | 0.184 | 4 | 0.005 |
| 20 | 0.1 | 0.184 | 6 | 0.001 |
| 20 | 0.1 | 0.184 | 6 | 0.005 |
| 20 | 0.1 | 0.184 | 6 | 0.010 |
| 20 | 0.1 | 0.184 | 8 | 0.001 |
| 20 | 0.1 | 0.184 | 8 | 0.005 |
| 20 | 0.1 | 0.184 | 8 | 0.010 |
| 20 | 0.1 | 0.184 | 8 | 0.020 |
| 20 | 0.1 | 0.184 | 10 | 0.001 |
| 20 | 0.1 | 0.184 | 10 | 0.005 |
| 20 | 0.1 | 0.184 | 10 | 0.010 |
| 20 | 0.1 | 0.184 | 10 | 0.020 |
| 20 | 0.1 | 0.184 | 10 | 0.030 |
| 20 | 0.1 | 0.184 | 12 | 0.001 |
| 20 | 0.1 | 0.184 | 12 | 0.005 |
| 20 | 0.1 | 0.184 | 12 | 0.010 |
| 20 | 0.1 | 0.184 | 12 | 0.020 |

The maximum soluble DSS amount was limited with the PVA concentration in the solutions due to the reasons that will be discussed in Chapter 4.

### 3.2.2 Size Measurements of Wormlike Micelles

Size measurements of the PVA shielded reverse micelle structures in the solutions were done after cooling to $25^0$C. Measurements were performed by using wide angle particle size analyzer. Initial temperatures of the solutions were ranging between 18 and $22^0$C. They were heated with a rate of $5\text{min}/^0$C and kept at $25^0$C for 10 minutes in the analyzer to establish the thermal equilibrium before the measurements. Solutions were contained in polystyrene cells during the measurements.

DLS technique was used to measure size of wormlike micelles in the solution. Measurements were done by using a wide angle particle size analyzer (Nanosizer ZS, Malvern Instruments Ltd., United Kingdom). The measurement range of the device was between 0.6 and 5000 nm. Samples were measured at $25^O$C, three sequential measurements was taken for each measurement. Particle size analysis equipment was shown in Figure 3.5. The device is connected to a computer and the results are taken by using DLS analysis software. The raw data of analyses are given in Appendix A.

**Figure 3.5** Particle size analysis equipment.

The solution having 0.068M $CuCl_2$, 12% PVA, and $3.37\times10^{-3}$M DSS, in which maximum micelle size was observed, was selected for the following experiments.

### 3.2.3 Electric Field Application to the Solution

For further increase in the average size of wormlike micelles, solutions were heated at different temperatures ranging between $25^0$C and $80^0$C, and an electric field (between 0 – 7 kV) was applied to the solutions. Experimental details and results are discussed in detail in Chapter 4. Schematic representation for the electric field application experiments is shown in Figure 3.6.

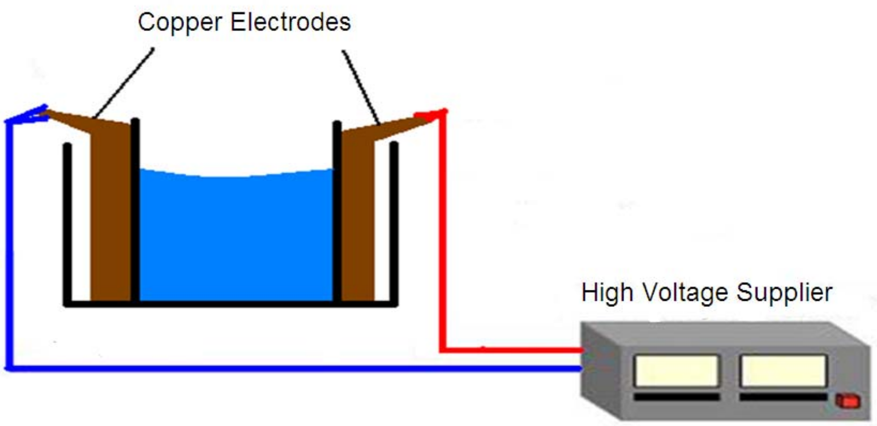

**Figure 3.6** Schematic representation of experimental setup.

The solution was contained in a PMMA (polymethylmethacrylate) cell and electric field was applied to the walls of the cell by copper electrodes. The cell is square shaped and 30 mm long. The wall thickness is 3 mm.

### 3.2.4 Reduction of Metal Ions

Different amounts of hydrazine hydrate were used to optimize the reduction reaction between Cu and hydrazine hydrate. The compositions of the solutions are given in Table 3.2.

**Table 3.2** Solution compositions for reduction experiments.

| $H_2O$(ml) | $NaHSO_3$ (g) | $CuCl_2$ (g) | PVA (%) | DSS (g) | $n_{Cu}/n_{HYD.}$ |
|---|---|---|---|---|---|
| 20 | 0.1 | 0.184 | 12 | 0.020 | 1:1 |
| 20 | 0.1 | 0.184 | 12 | 0.020 | 1:2 |
| 20 | 0.1 | 0.184 | 12 | 0.020 | 1:2.5 |
| 20 | 0.1 | 0.184 | 12 | 0.020 | 1:3.5 |
| 20 | 0.1 | 0.184 | 12 | 0.020 | 1:5 |
| 20 | 0.1 | 0.184 | 12 | 0.020 | 1:7.5 |
| 20 | 0.1 | 0.184 | 12 | 0.020 | 1:10 |

### 3.2.5 Electrospinning of the Solution

The electrospinning setup was consisted of a direct current (DC) high voltage supply, syringe pump, and the collector as shown in Figure 3.7. DC voltage supply (ES30P-20W/DAM GAMMA High Voltage Research Inc., USA) had an electrical potential range between 0 and 30 kV. The feed rate of the solution was regulated by using a six channel syringe pump (NE-1600 Six-Syringe

Pump, New Era Pump Systems Inc.). The flowrate of syringe pump could be varied between 0.568 μL/h (1 ml syringe) and 1337 ml/h (60 ml syringe). In this study, a 10 ml syringe (Ayset A.Ş., Türkiye) with a needle diameter of 0.8 mm was used and the voltage was applied between the tip of the syringe and grounded collctor. Electrospun fibers were collected on a metal collector covered with aluminum foil. Electrospinning setup was kept in a PMMA (polymethylmethaclyate) container due to the safety considerations. The solutions were electrospun for two hours in all the electrospinning experiments. The setup of electrospinning is illustrated in Figure 3.7.

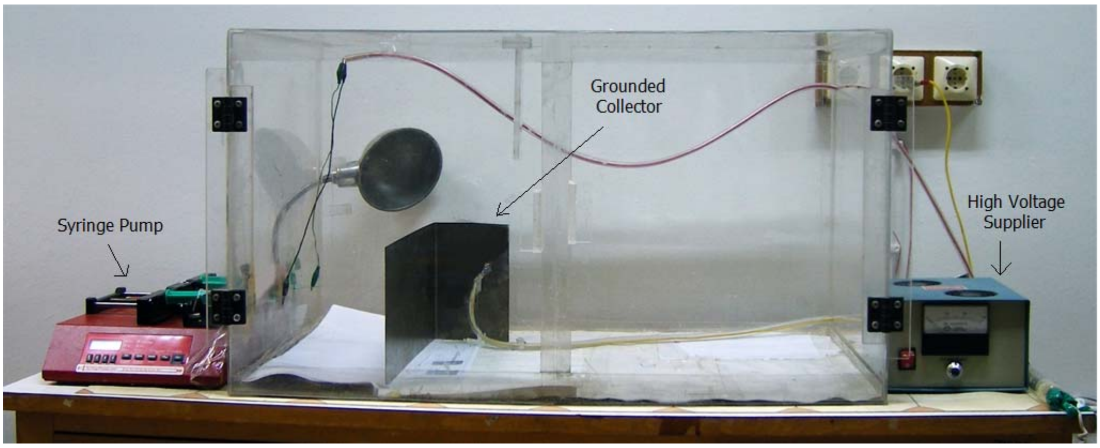

**Figure 3.7** Photograph of electrospinning setup used in this study.

Morphology characterization of the electrospun fibers was done by using SEM (Quanto 400F - Fei Field Emission Gun). In order to distinguish Cu from PVA, the majority of SEM images were taken in backscatter mode, in which number of scattered electrons from an element is proportional with its molecular weight. Elemental analyses of nanofibers were done by using Energy Dispersive X-Ray Analysis (EDX) probe of SEM. Samples were sputtered with 4 nm of Au before SEM analysis.

The schematic representation of the experimental procedure is shown in Figure 3.8.

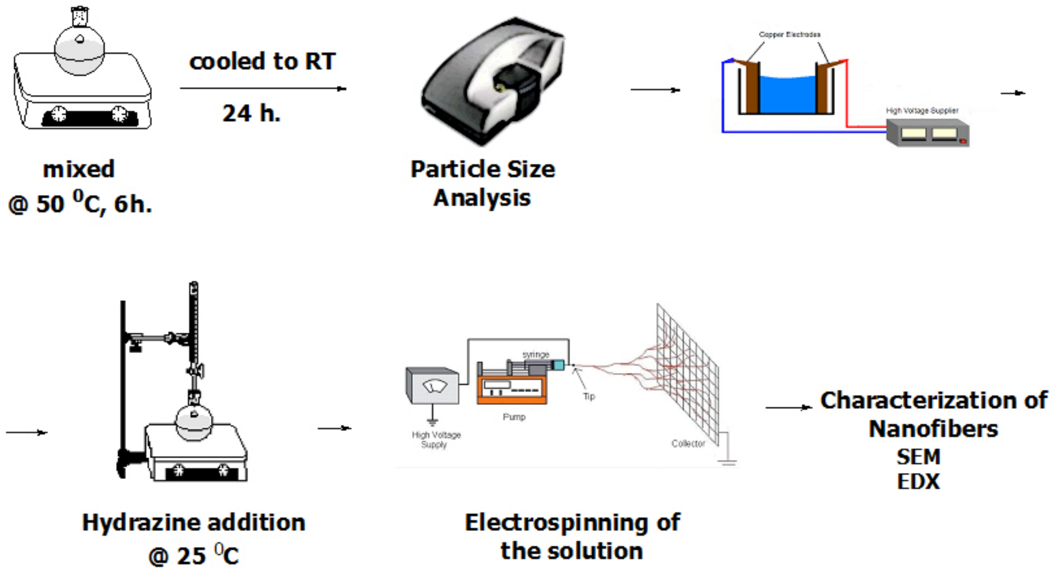

**Figure 3.8** Experimental procedure.

The solutions were prepared under magnetic stirring at 50 $^0$C. The size measurements were performed at room temperature and electric field was applied to the solutions in order to increase the average size of micelles. Hydrazine hydrate was added to the solution dropwise by using a titration burette. The morphological characterization of the nanofibers was done by SEM after electrospinning.

# CHAPTER 4

# RESULTS AND DISCUSSIONS

In this chapter, in the light of SEM micrographs, experimental results and discussions are presented. The general route of solution preparation and reduction experiments was determined with preliminary experiments. Wormlike micelle formation and size analyses of the micelle formation are investigated in Section 4.2. Effect of electric field and heating on reverse wormlike micelle formation is discussed in Sections 4.2.3 and 4.2.4. The optimization of the reduction reaction is done in Section 4.3., while the size and morphology analyses of electrospun fibers are presented in Sections 4.3 and 4.4.

## 4.1 Preliminary Results

### 4.1.1 Solution Preparation

First of all, the solution composition was adjusted to prepare a solution without precipitation in which, the micelle structures are suspended. To achieve this, the amounts, and the order of addition of the chemicals were determined in the preliminary experiments. Different addition orders were tried to examine the effect of chemicals on micelle formation. Four different compositions were investigated for the determination of the most appropriate one. These four compositions are summarized in Table 4.1.

*Composition 1 (R1)* : 0.068M $CuCl_2$, and $3.37\times10^{-3}$M DSS was dissolved in 20 ml deionized water at room temperature under vigorous stirring. After having a homogeneous solution, 2.4g PVA was added to the solution under stirring. Homogeneous solution was observed after stirring 24 h at room temperature.

*Composition 2 (R2)* : 0.068M $CuCl_2$, and $3.37\times10^{-3}$M DSS was dissolved in 5 ml deionized water and 2.4g PVA was dissolved in 15 ml deionized water. Both solutions were homogeneous after stirring for 24 h at room temperature. Then, two solutions were mixed under stirring and a homogeneous solution was observed.

*Composition 3 (R3)* : 0.068M $CuCl_2$, 2.4g PVA, and $3.37\times10^{-3}$M DSS was dissolved in 20 ml deionized water. After mixing for 24 h, the solution became homogeneous.

*Composition 4 (R4)* : 0.068M $CuCl_2$, 2.4g PVA, and $3.37\times10^{-3}$M DSS was dissolved in 20 ml deionized water. Homogeneous solution was observed after mixing for 4 h at 75 $^{O}$C. The composition was the same as R3, but the mixing was done at 75 $^{O}$C.

Precipitation was observed in the solutions R1 and R2. During formation of wormlike micelles, the anionic head of the surfactant interacts with $Cu^{2+}$ ions and micelles are formed. $Cu^{2+}$ was in the core and surrounded by surfactant molecules. Hydroxyl groups of PVA should have interacted with the hydrophobic tail of the surfactant. This interaction leads PVA surround the micelle structure to keep the micelle structure suspended. When it was added afterwards, it interacts with water molecules instead of the surfactant molecules resulting in the precipitation. The precipitate was placed on a lamella and dried for 24 h at 60 $^{O}$C for analysis. The morphology of the precipitates can be seen in the SEM micrographs of the sample shown in Figure 4.1.

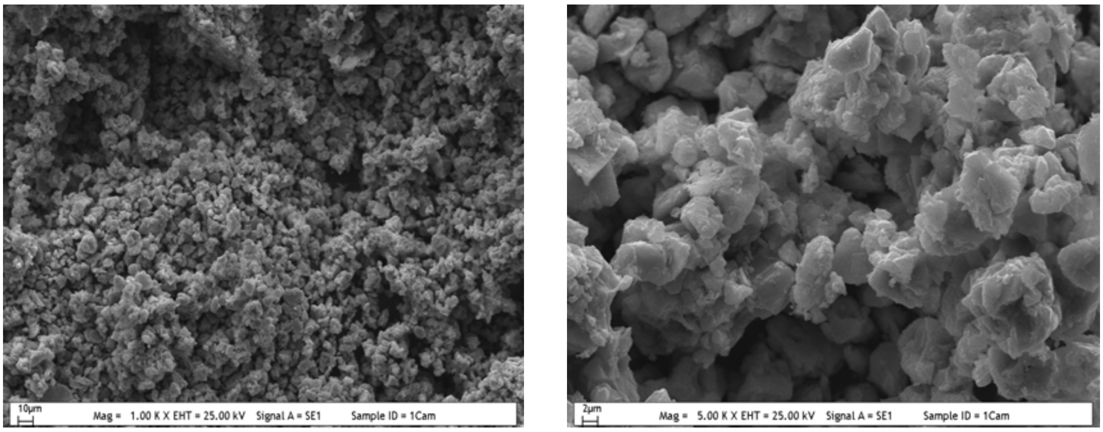

**(a)** **(b)**

**Figure 4.1** SEM micrographs of precipitated sample prepared by using R1. **(a)** ×1000 magnification; **(b)** ×5000 magnification

On the other hand, the solutions prepared with compositions R3 and R4 were found to be homogeneous without any precipitation. The preparation of R4 is quicker than that of R3, therefore it is used in the rest of the study.

### 4.1.2 Preliminary Reduction Experiments

Hydrazine hydrate was used as the reducing agent to reduce Cu ions in the solution. Similar to the solution preparation step, some preliminary experiments were performed to investigate the reduction reaction. In order to determine the proper reaction temperature, two different reaction temperatures were investigated. The color change of the solution was faster when the solution temperature was increased to 40°C. The reaction was accelerated by increasing the solution temperature as expected. It was hard to investigate the effect of variables on reduction at high temperature; therefore the experiments were carried out at 25°C, where the color change was much slower than at 40°C. In the early reduction experiments CuO was observed instead of metallic Cu. The color of the solution turned into black which is the color of copper oxide. It was suspected that oxygen dissolution in water could cause the oxidation of Cu nanoparticles. Two different methods were investigated to prevent oxidation reaction.

Deionized water was boiled to remove any dissolved oxygen and cooled back to 25°C in a closed container. The method was successful for high ratios of copper to hydrazine hydrate, i.e., 1:1 and 1:2.5. The oxidation of copper could not be prevented if the molar ratio was decreased to 1:5 or below. The color of the solution was turned into black for this condition. As the reaction temperature was increased to 40°C, the color of the solution was turned into black even with the ratio of 1:2.5. Therefore, the following reduction experiments were carried out at room temperature.

In literature, sodium bisulfite ($NaHSO_3$) was commonly used to remove dissolved oxygen in water. The sulfite ion binds oxygen molecule and sulfate ions were produced. The proposed reaction mechanism for the removal of oxygen was given by Asano et al.[49] and presented in Equation 4.1.

$$2HSO_3^- \text{ (aq)} + O_2 \text{ (gas)} \rightarrow SO_4^{2-} \text{ (aq)} + H_2 \text{ (gas)} \qquad (4.1)$$

Following the addition of $NaHSO_3$, it was observed that the color of Cu nanoparticles did not turn into black indicating the prevention of oxidation. The optimum amount of $NaHSO_3$ was determined experimentally. The optimum amount of $NaHSO_3$ was found to be 0.048 M.

### 4.1.3 Parametric Study of Electrospinning

Electrospinning is a very simple but sophisticated technique to produce polymeric nanofibers. To obtain beadless and continuous fibers, the solution viscosity, the surface tension, and the applied voltage should be delicately adjusted. To identify the appropriate electrospinning conditions, different solutions were electrospun. Electrospinning parameters that are investigated in this study are summarized in Table 4.1.

**Table 4.1** Electrospinning conditions.

| **PVA % (w/v)** | **Feed Rate (ml/h)** | **Applied Voltage (kV)** |
|---|---|---|
| 8 | 0.8 | 12 |
| 8 | 0.8 | 16 |
| 8 | 0.8 | 20 |
| 8 | 1.0 | 16 |
| 6 | 0.8 | 16 |

The applied voltage was 12 kV, electrospinning could not be accomplished, because the force created by electric field was not sufficient enough to overcome the surface tension of the liquid. This resulted in the formation of droplets without the fiber form. Upon the increase of the voltage to 20 kV, the instability at the tip of syringe was so high that the uniform production of fibers could not be achieved again. There was even tiny sparks from the tip to the syringe pump. The surface tension of the liquid was insufficient to balance the applied voltage. With the feed rate of 0.8 ml/h, the optimum value of applied voltage was found to be 16 kV to obtain beadless and continuous nanofibers. If the polymer content of the solution was decreased to 6%, beaded fibers were formed; because, the surface tension of the liquid was not sufficient to permit the stretching of fibers. The feed rate was increased to 1 ml/h, there was not sufficient time for solvent evaporation. Collected fibers were still wet. The morphologies of electrospun fibers with different electrospinning conditions are shown in Figure 4.2.

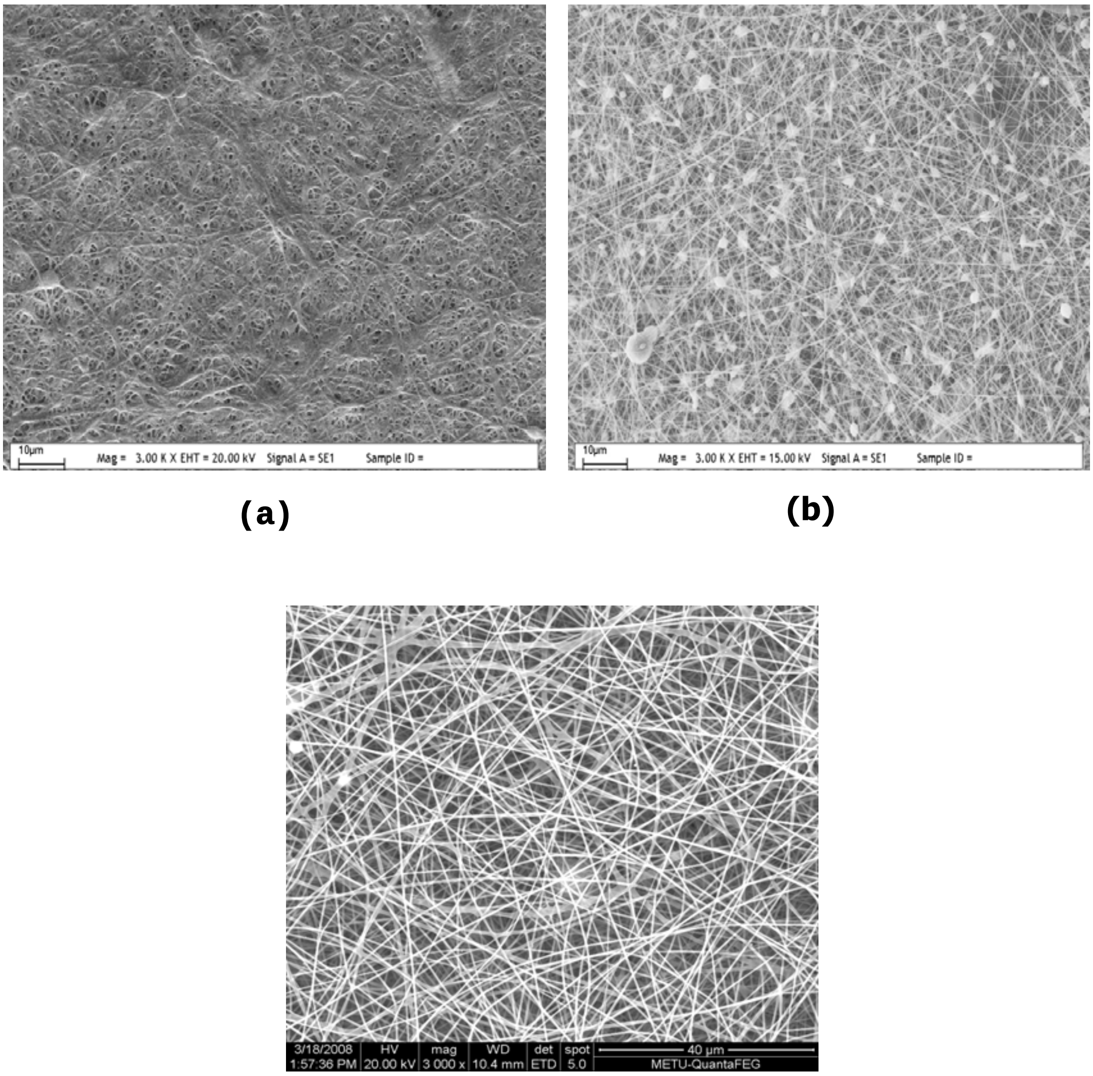

**(a)** **(b)**

**(c)**

**Figure 4.2** SEM images of electrospun nanofibers (a) 8% PVA, 1ml/h, 16 kV; (b) 6% PVA, 0.8 ml/h, 16 kV; (c) 8% PVA, 0.8 ml/h, 16 kV.

Following the preliminary experiments, the parameters affecting wormlike micelle formation were investigated and optimum ratios were determined for the formation of the wormlike micelle. In the rest of experiments the electrospinning parameters were adjusted as; feed rate: 0.8 ml, voltage: 16 kV, tip-to-collector distance: 15 cm.

## 4.2 Wormlike Micelle Formation in the Solution

The wormlike micelle structure was established by using $Cu^{2+}$, DSS and PVA. The representative figure of the reversed wormlike structure is given in Figure 4.3.

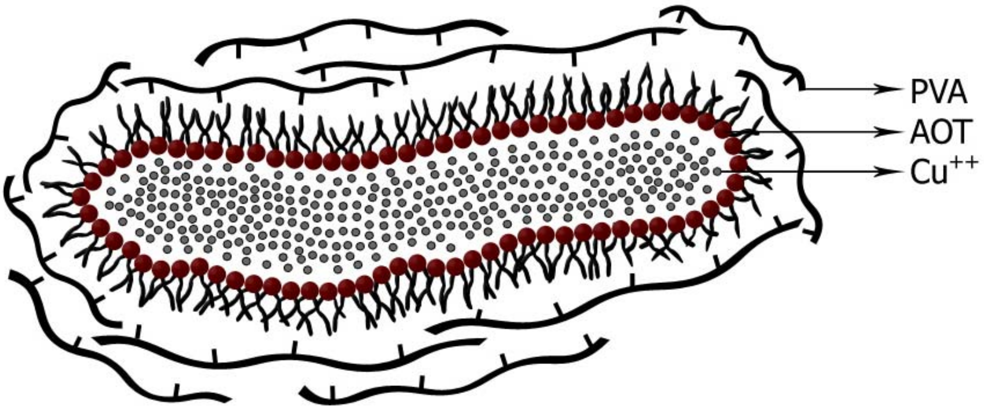

**Figure 4.3** Schematic representation of reversed wormlike micelle structure.

Solutions with different compositions were prepared to determine the effect of molar ratios on the wormlike micelle structure. Increasing the amount of $CuCl_2$ decreased the surface tension of the solution leading to failure in electrospinning. The surface tension of the solution was not able to balance the applied electric field force. Because of this observation, the amount of

$CuCl_2$ was not increased further. The maximum allowable $CuCl_2$ was used in the experiments.

The amounts of $CuCl_2$ and $NaHSO_3$ were kept constant and solutions having different amounts of PVA were prepared. DSS concentrations ranging between $1.13\times10^{-4}$M and $3.37\times10^{-3}$M were added to the solutions. The compositions of prepared solutions are summarized in Table 4.2.

**Table 4.2** Compositions of the solutions for micelle formation.

| $H_2O$ (ml) | $NaHSO_3$ (g) | $CuCl_2$ (g) | PVA (%) | DSS (g) | Mixing Time (h) |
|---|---|---|---|---|---|
| 20 | 0.1 | 0.184 | - | - | 24 |
| 20 | 0.1 | 0.184 | 4 | 0.005 | 6 |
| 20 | 0.1 | 0.184 | 6 | 0.010 | 6 |
| 20 | 0.1 | 0.184 | 8 | 0.020 | 6 |
| 20 | 0.1 | 0.184 | 10 | 0.030 | 6 |
| 20 | 0.1 | 0.184 | 12 | 0.020 | 6 |

The maximum amount of soluble DSS was also dependent on PVA concentration. Without the presence of PVA, DSS molecules coagulated on $Cu^{2+}$ molecules. In the reverse wormlike micelle structure, the hydrophilic heads of DSS are directed towards inner part of the micelle, and hydrophobic tails of DSS are directed towards outside. Without the shielding effect of PVA, the motion of DSS molecules was too fast and micelle structures precipitated. Anionic head of DSS is strongly attracted by the positive charge on $Cu^{2+}$ and the coagulation of hydrophobic tails caused phase separation followed by precipitation. With the increasing PVA concentration, PVA interacts with the hydrophobic tail of the surfactant and acts as a shield on the micelle structure. It, in turn, provides stability, and so PVA prevents the coagulation of DSS surrounded $Cu^{2+}$ micelles. The amount of soluble DSS increased with increasing PVA concentration as shown in Table 4.1.

In thick solutions with 12% PVA, the DSS could be increased to $3.37\times10^{-3}$M. However, it imparted high opacity, and DLS measurements could not be performed.

To optimize the amount of DSS and PVA for micelle formation, different amounts of DSS and PVA were added to the solutions while amounts of other chemicals were kept constant in the following experiments.

### 4.2.1 Effect of the Amount of DSS Amount on Wormlike Micelle Formation

As reported by Wu et al.[21] wormlike micelle formation depends on the surfactant concentration. Micelles in the solution will grow with increasing surfactant concentration. Wormlike micelle structures are observed when the surfactant concentration is about 15 times of the CMC.

In order to investigate the formation of micelle structures in the solution, different amounts of DSS ranging from $1.13\times10^{-4}$ M to $3.37\times10^{-3}$ M were added to the solutions, keeping amounts of all other chemicals constant. The results are tabulated in Figure 4.4. Raw data of the size measurements are presented in Appendix A.

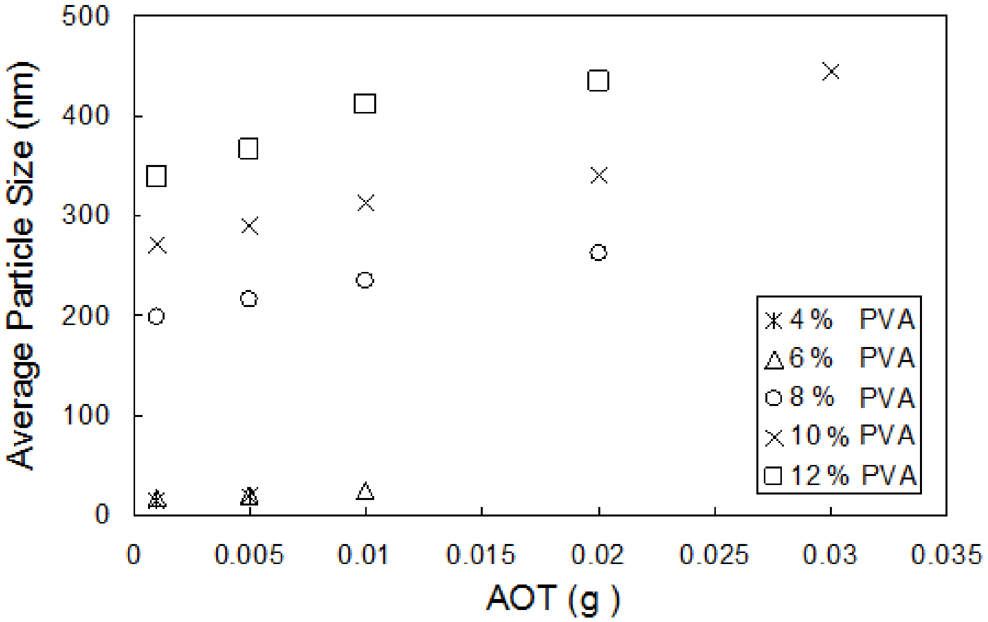

**Figure 4.4** Effect of DSS concentration on size of wormlike micelles.

It is seen from Figure 4.4 that average particle size increases with the increase in surfactant concentration. The increase in the amount of surfactant increases their mutual interaction, and thus fusion of micelles. The more the surfactant molecules in the solution, the larger wormlike micelle structures are observed.

As explained earlier, the number of micelles suspended in the solution is also dependent on the amount of PVA. Figure 4.4 also shows that as the PVA content increases larger micelles can suspend in the solution, so the amount $Cu^{2+}$ that held in the micelles increased.

For the solutions having 4% and 6% PVA, the maximum amount of soluble DSS was below the CMC of DSS. Below CMC, the interaction between the surfactant molecules was very low and micelle structure was not formed.

Only a few of the surfactant molecules can interact with each other resulting in very low particle size as compared to the solutions having 8%, 10% and 12% PVA.

There were restrictions for the precise measurement of micelle size when DSS concentration was further increased for the solution with 12% PVA. The two prevailing effects were the tremendous increase of opacity which limits the precision of optical measurements, and the loss of random Brownian motion of micelles.

### 4.2.2 Effect of the Amount of PVA on Wormlike Micelle Formation

For the solutions with different DSS concentrations, during the size measurements, it was noticed that the amount of PVA also strongly affects the size of the reverse micelles. In the absence of PVA, reverse micelle structures could not be suspended in the solution and precipitation was observed in the solution.

In order to clarify the effect of PVA on reverse micelle formation, solutions with different PVA content ranging from 4% to 12% was prepared keeping the amounts of all other chemicals constant. The results are summarized in Figure 4.5 and the raw data of size measurements are presented in Appendix A. As shown in Figure 4.5 the average particle size of the micelles increased with the increasing concentration of PVA. The increase of PVA provided sufficient stability for the suspension of the wormlike micelle structures.

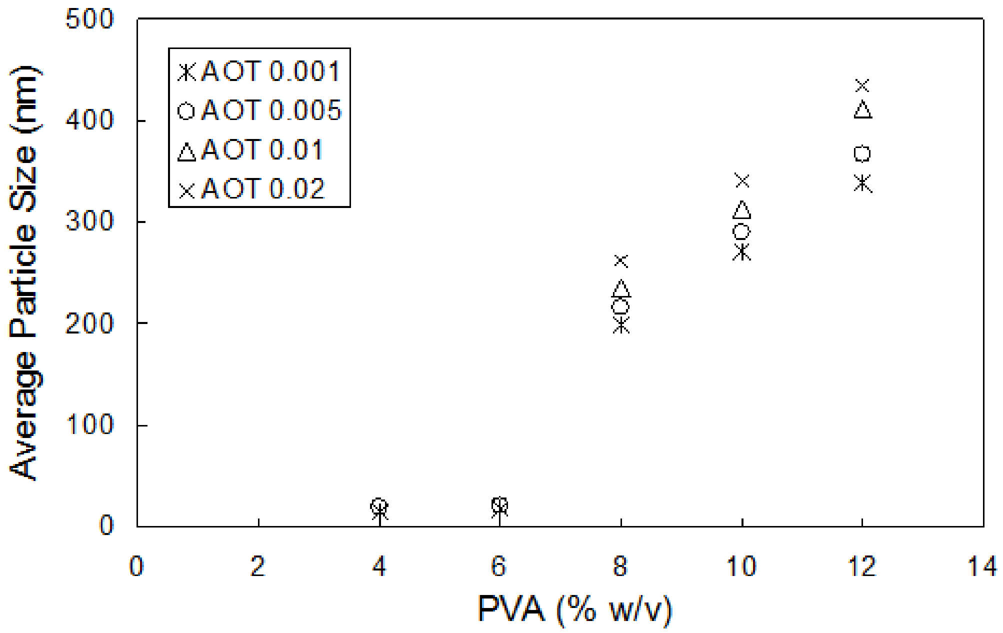

**Figure 4.5** Effect of PVA concentration on size of wormlike micelles.

PVA plays two major roles in the formation of the reversed wormlike micelle formation. First, it interacts with the hydrophobic tail of the surfactant and functioning as a shield it keeps the micelle structure together. Due to this shielding effect, the interactions of surfactant molecules with other surfactant molecules that are present in other wormlike micelles were stabilized such that they interact without coagulation. If the interaction was not controlled, the hydrophobic tails of the surfactant molecules could fuse and led to phase separation in the solution. Second, following the reduction of Cu ions, the surfactant molecules tend to leave the micelle structure. Although there might be still very weak interaction between the sulfur end of micelle and metallic copper, it is far from being sufficient to hold the surfactant molecules together. However, PVA can keep them together because of the large increase of viscosity. The effect of PVA on solution viscosity was investigated for the solutions having from 4% to 12% PVA and results are shown in Figure 4.6.

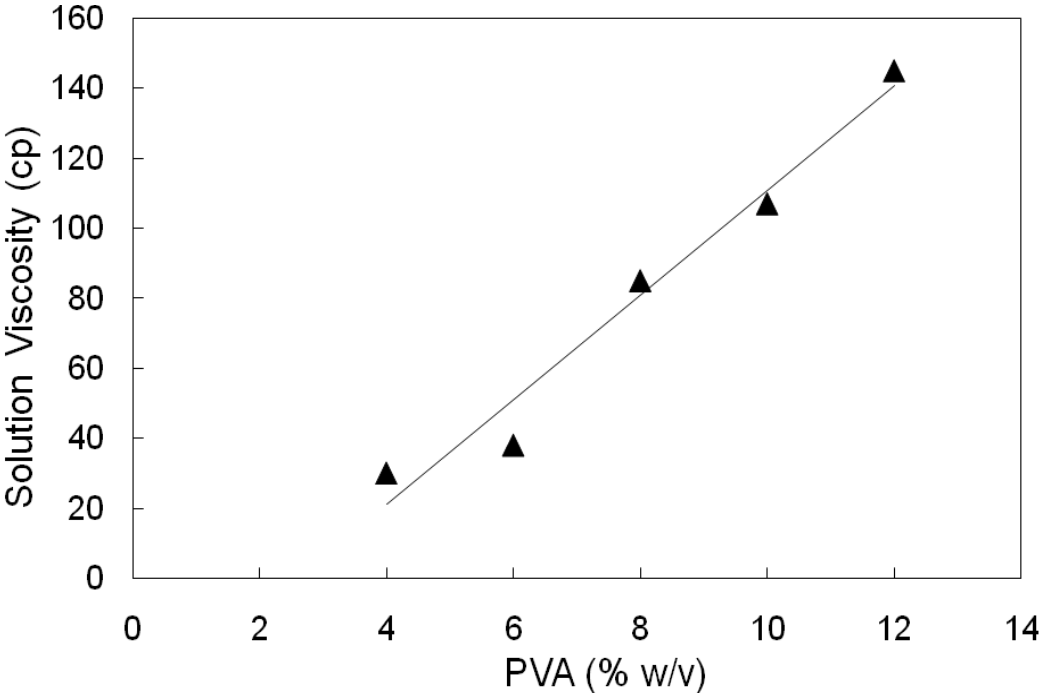

**Figure 4.6** Effect of PVA concentration on solution viscosity ($C_{DSS}$=0.0050g/ml).

The viscosity of the solution was found to be dependent on PVA concentration. The concentration of PVA was increased above 12%, the fluidity of the solution decreased tremendously and the syringe pump could not feed the solution with at a constant rate. Under these conditions, electrospinning experiments could not be carried out. There is also a lower limit for the concentration of PVA. For the solutions with a PVA concentration less than 7%, the solution viscosity was found to be very low for the realization of electrospinning.

It can be deduced from Figure 4.4 and 4.5 that the size of the wormlike micelle and the interaction between DSS and $Cu^{2+}$ were maximized in the solution having $2.25\times10^{-3}$ M DSS and 12% PVA. The maximum achieved size of the wormlike micelles was about 435 nm. Other additional parameters were investigated for a possibility of a further increase the size of the micelles.

### 4.2.3 Effect of Heating on Size of the Wormlike Micelles

Another parameter that may increase the size of micelles is temperature. The kinetic energy of the particles in a solution would increase with temperature; the collision of micelles can cause their fusion with each other leading to a size increase. In order to investigate the effect of temperature on micelle formation the solutions were heated to 4 different temperatures, namely, 40°C, 60°C, and 80°C for 4 hours. Particle size measurements were then performed results of which are summarized with their standard deviation values in Table 4.3.

**Table 4.3** Effect of heating on wormlike micelle size.

| Temperature of the Solution (°C) | Average Particle Size (nm) |
|---|---|
| 25 | 436.2±129 |
| 40 | 444.6±139 |
| 60 | 500.6±111 |
| 80 | - |

For the solutions that are heated to 80°C, precipitation was observed due to the coagulation of the micelles. Coagulations naturally changed size measurements. The main reason for the precipitation could be the behavior of PVA at this temperature. The chains of PVA will be more relaxed and move randomly in the solution at high temperatures. It can interact with water molecules rather than the surfactant molecules. Without the shielding effect of PVA, the reversed micelle structures may tend to invert the surfactant molecules to decrease the free energy content of the solution. The presence of Cu ion prevents the inversion of the micelle structures and the hydrophobic tails of the surfactant molecules interact and cause phase separation. It was seen that increasing the solution temperature did not result in a considerable increase in the size of the reversed wormlike micelles.

### 4.2.4 Effect of Electric Field on Size of the Wormlike Micelles

Cu ions are present in the center of the wormlike micelles. It could be possible to align metal ions under electrical field, which in turn align micelles. this could then be followed by coagulation and increase the length of wormlike micelle. In order to investigate the validity of this thought the solution was kept under high electrostatic field prior to electrospinning.

Two different voltages namely, 5 and 7 kV were applied to the solution for 4 hours. The size of wormlike micelles increased up to 644 nm with the application of electric field. The results observed in these experiments were summarized in Figure 4.7. The size of the micelles increased linearly with the voltage.

These solutions were also electrospun to see the effect of the size increase due to electrostatic field on nanofiber morphology. The morphology of fibers is examined by SEM and the results are shown in Figure 4.8.

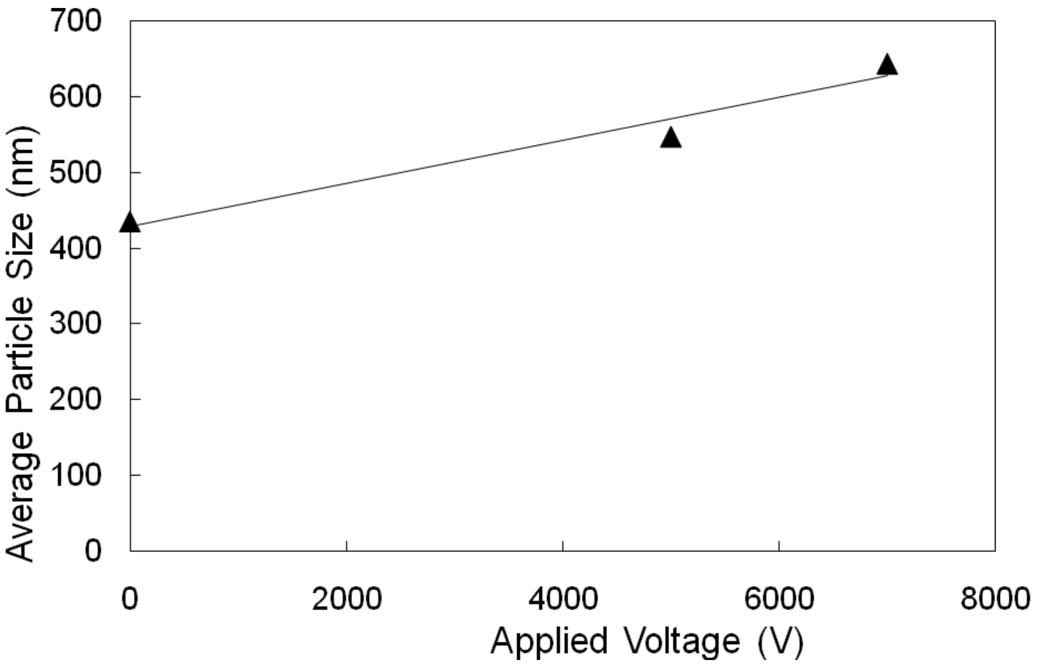

**Figure 4.7** Effect of electric field on size of wormlike micelles.

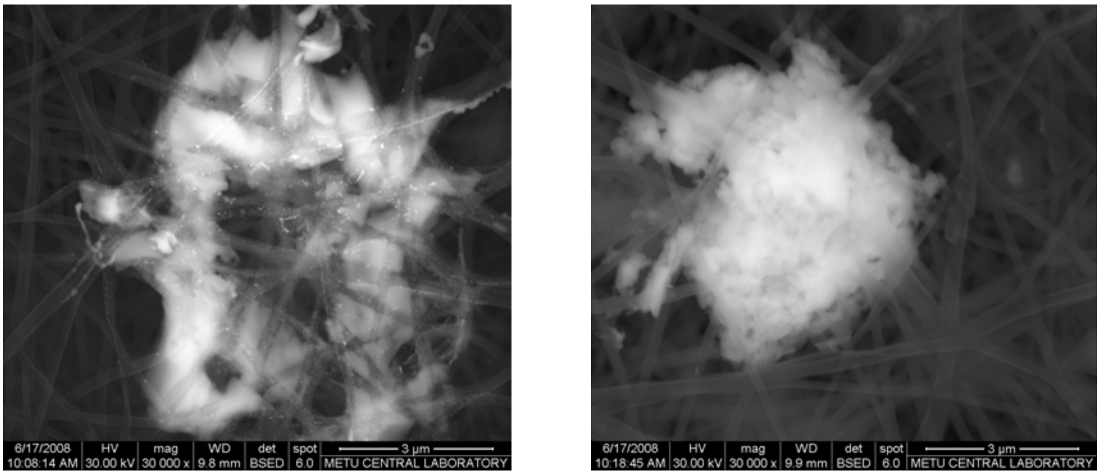

**(a)** **(b)**

**Figure 4.8** SEM micrographs of 4 hours electric field applied nanofibers **(a)** 5 kV; **(b)** 7 kV.

Figure 4.8 shows that there are large copper deposits that are randomly distributed on the nanofiber mat. The electrostatic field might have caused heavy coagulations yielding large deposits. In other words large micelles could not be distributed in nanofibers. This effect was observed clearly in both voltages in Figure 4.8.

Consequently, the samples were kept under electrostatic field for 1 hour. The applied voltage was also reduced to 3 and 5 kV. The average particle size of wormlike micelles was then measured as 465.6±121 nm for 3 kV, and 518.3±151 nm for 5 kV, respectively. The morphology of electrospun fibers following the application of 3 and 5 kV are shown in Figure 4.9 (a) and (b) respectively.

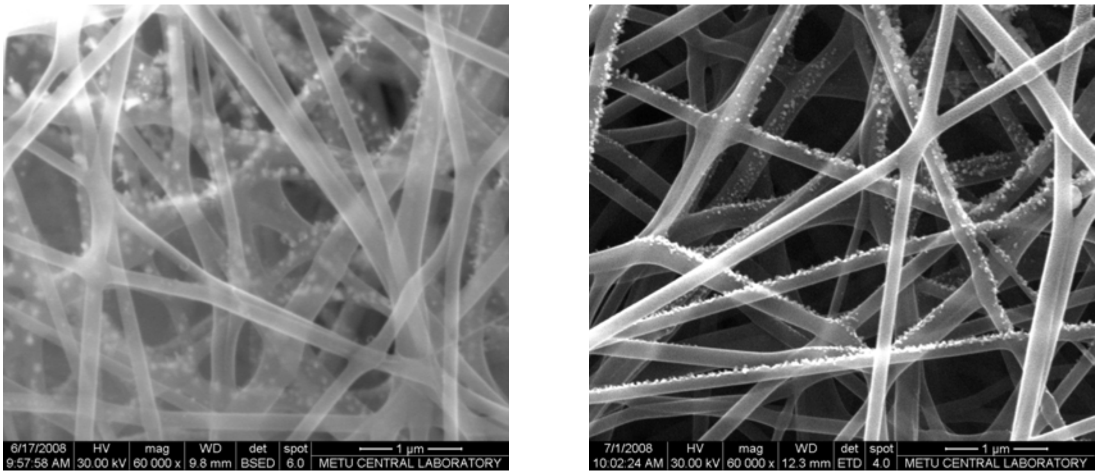

**(a)** **(b)**

**Figure 4.9** SEM micrographs of 1 hour electric field applied nanofibers **(a)** 3 kV; **(b)** 5 kV.

Large deposits that were observed fo the samples at 5 and 7 kV were disappeared as shown in Figure and 4.9 (a) and (b). The Cu nanoparticles attached to the surface of fibers can be clearly observed in Figure 4.9b.

To investigate the common effect of electric field and heating, different solutions were prepared, which were heated to 25°C, 40°C, and 60°C. The electric field was applied as 1 kV, 3 kV, and 5 kV for one hour to the solutions after heationg. The combined effect of electric field and heating is seen in Figure 4.10.

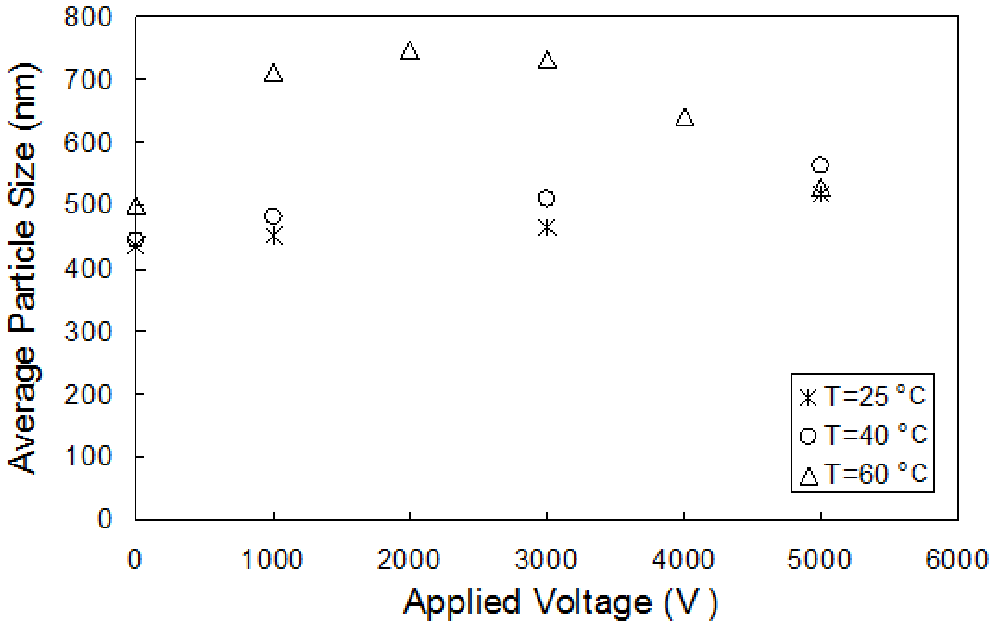

**Figure 4.10** Combined effect of electric field and heating on the average size of the wormlike micelles.

The change in the average particle size was not appreciable change when the temperature was increased from 25°C to 40°C. In case of heating to

60°C, the particle size first increased up to 2 kV and then decreased with the increasing voltage. It was observed in the experiments that the applied electric field caused coagulation of Cu nanoparticles followed by precipitation. So the device could measure only the remaining small sized particles.

The average size values at 5 kV of the three samples were almost the same, which showed that maximum size of the wormlike micelles that can be suspended in 12% PVA solution was about 530 nm. However, when the size of the wormlike micelles was above about 450 nm, metal nanoparticles could not be distributed homogeneously, they yielded large deposits.

## 4.3 Reduction of Copper Ions

Hydrazine hydrate was used as the reducing agent for the reduction of Cu ions. As discussed in Chapter 2, hydrazine hydrate was used to reduce a variety of metals. By considering previous works in literature, the expected reaction mechanism can be given as:

$$N_2H_5^+ + 2Cu^{2+} + 5OH^- \rightarrow N_2 + 2Cu + 5H_2O \qquad (4.1)$$

According to the given mechanism one mole of hydrazine hydrate is expected to reduce two moles of $Cu^{2+}$. Excess hydrazine hydrate is used to shift the reaction to the right in the literature. The reaction was not expected to go to completion since it takes place in a viscous solution. Diffusion of hydrazine hydrate is slow in the solution and some of the hydrazine hydrate molecules are not able to come across with Cu ions.

The reaction could not go to completion due to the insufficient mixing, when hydrazine hydrate was added to the solution without dilution. The solution viscosity was measured to be as high as ~145 cP preventing the diffusion of hydrazine hydrate molecules into the micelle structures.

Hydrazine hydrate is a very powerful reagent and its -$NH_2$ groups form hydrogen bonds with PVA and with the hydrophobic tail of DSS. It, in turn, tends to destroy the wormlike micelle structure. In order to ease the diffusion of hydrazine hydrate and provide mixing thoroughly hydrazine hydrate was diluted in 10 ml of DI water before adding to the solution.

In order to find the optimum amount of hydrazine hydrate for the reaction, hydrazine hydrate was added to the solution with different Cu to hydrazine hydrate ratios.

### 4.3.1 Reduction with Prompt Hydrazine Hydrate Addition

Hydrazine hydrate was added to the solutions instantaneously by pouring from the beaker. When the molar ratio of copper to hydrazine hydrate was 1, reduction reaction could not be completed. The color of the solution was green, which was almost the same as the color of the starting solution containing $Cu^{2+}$ ions.

Afterwards, the ratio was decreased to 1:2, the color of the solution was yellow, which is identified as the color of $Cu^{+}$ [50]. The reduction reaction could not go to completion; $Cu^{++}$ was reduced to $Cu^{+}$. Thus, the amount of hydrazine hydrate was further increased to achieve completion of reaction.

For the ratios 1:2.5, 1:5, and 1:10 the color of the solution was bronze/brown, and it did not change with an increase in the amount of hydrazine hydrate. This clearly indicates the completion of the reaction. The solutions were then electrospun to obtain nanofibers and the morphology of Cu nanoparticles was investigated. Figure 4.11 shows the morphology of the nanofibers on prompt addition of hydrazine hydrate to the solution.

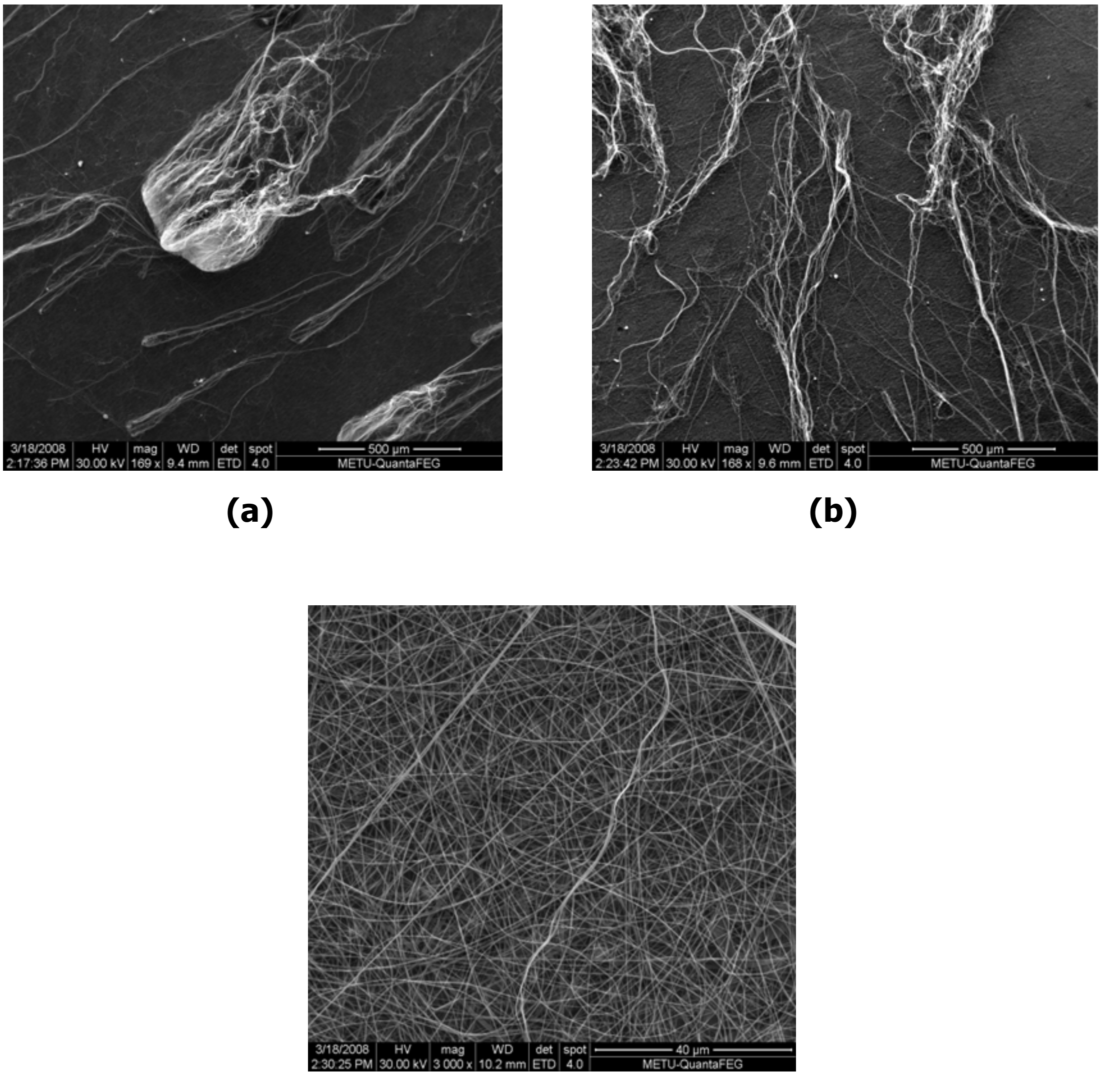

**(a)** **(b)**

**(c)**

**Figure 4.11** SEM micrographs of nanofibers with Cu to hydrazine hydrate ratios **(a)** 1:10; **(b)** 1:5, **(c)** 1:2.5.

Although the reduction reaction was completed, copper nano particles did not stay in PVA shield. At high hydrazine hydrate concentrations the fiber morphologies also destructed as seen from Figure 4.11 (a) and (b). The $-NH_2$ groups of hydrazine hydrate can form relatively strong hydrogen bonds with PVA. As a result of this interaction, PVA was not able to interact with the hydrophilic tails of the DSS molecules. The schematic for the interaction between hydrazine hydrate and PVA is shown in Figure 4.12.

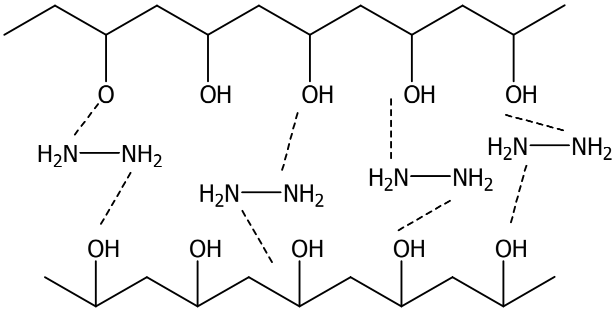

**Figure 4.12** The interaction between hydrazine hydrate and PVA.

For the ratio 1:2.5, the amount of hydrazine hydrate was relatively low, and continuous fibers were produced as seen from Figure 4.11 (c). Continuous PVA nanofibers were produced; however, Cu nanoparticles could not be distributed in PVA. Instantaneous addition of hydrazine hydrate did not destruct the morphology of PVA, but it destructed the wormlike micelle structure and Cu nanoparticles ran out of the PVA shield during electrospinning.

Upon addition, hydrazine hydrate will immediately react with the molecules at the surface of the solution. Because of the high viscosity, diffusion of hydrazine hydrate molecules towards Cu ions would be difficult. Even at low hydrazine hydrate concentrations the micelles at the surface confronted with excess amount of hydrazine hydrate on prompt addition destroying the micelle structure.

### 4.3.2 Reduction with Stepwise Hydrazine Hydrate Addition

In order to minimize the adverse effects of hydrazine hydrate on the micelle structures, hydrazine hydrate addition rate was decreased to 0.25 ml/min, and the following experiments were done at this addition rate. Continuous nanofibers could be obtained a Cu/hydrazine hydrate ratio of 1:5, however, Cu nanoparticles left the micelle structure, and coagulated. The unpaired electrons of nitrogen can also interact with the unpaired electrons of Cu. High interaction capacity of -$NH_2$ groups with metal ions, hydrazine hydrate was also used in the literature to produce size-controlled metal nanoparticles [17, 30], because, □$NH_2$ groups of hydrazine hydrate can easily interact with the outer shell electrons of metals. The schematic representation of the interaction between hydrazine hydrate and Cu nanoparticles is shown in Figure 4.13.

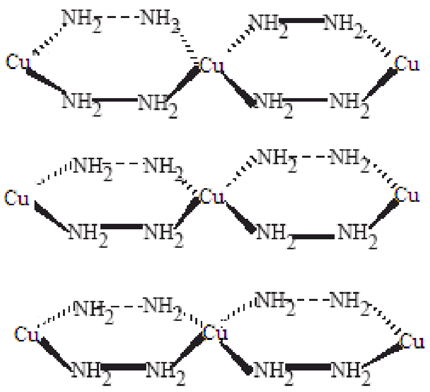

**Figure 4.13** Schematic representation of the interaction between hydrazine hydrate and Cu nanoparticles.

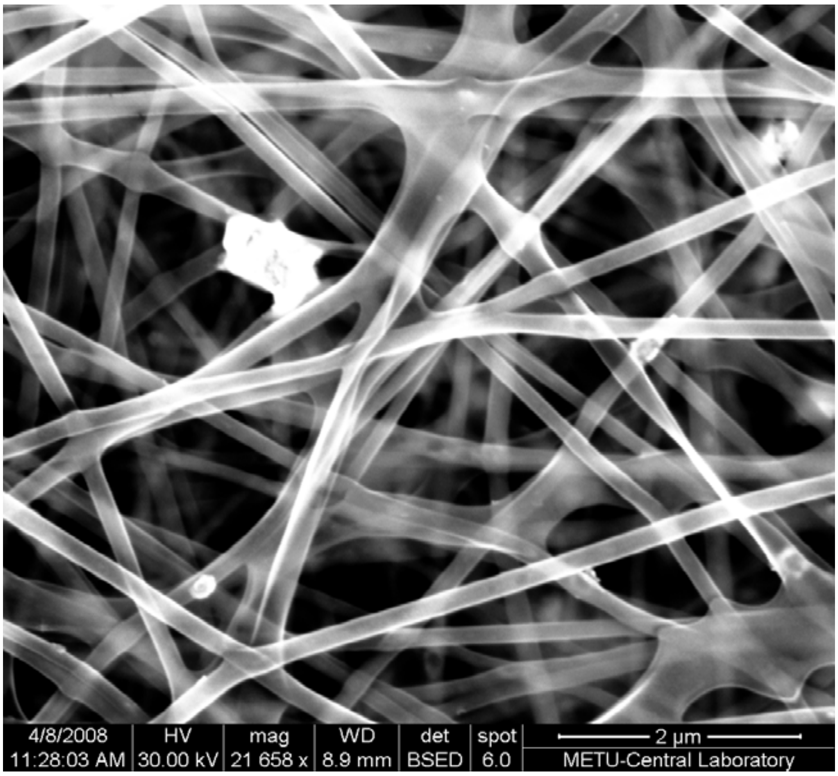

**Figure 4.14** SEM micrograph of nanofibers with a Cu to hydrazine hydrate ratio of 1:5 (V:16 kV, d:15 cm, feedrate:0.8ml/h).

The morphology of the electrospun fibers obtained from the solution having 1:5 copper to hydrazine hydrate ratio is shown in Figure 4.14.

The molar ratio of Cu to hydrazine hydrate was further increased and the bridging effect of hydrazine hydrate was partly prevented by decreasing the excess amount of hydrazine hydrate. Smaller coagulations of copper nanoparticles were observed at the molar ratio of 1:3.5. The morphology of nanofibers is shown in Figure 4.15.

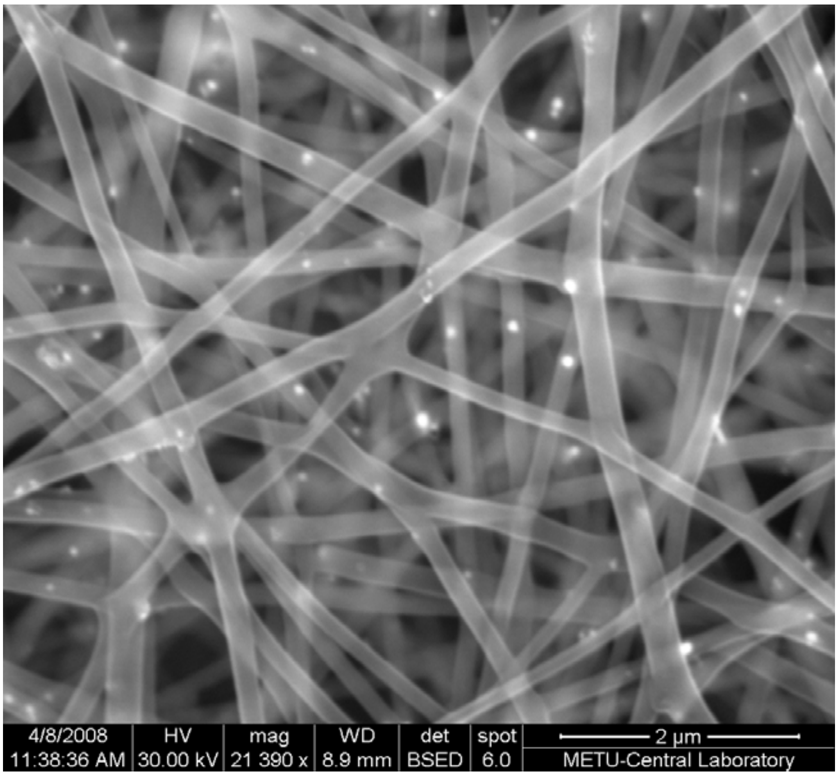

**Figure 4.15** SEM micrograph of nanofibers with a Cu to hydrazine hydrate ratio of 1:3.5 (V:16 kV, d:15 cm, feedrate:0.8ml/h).

With the ratio of 1:2.5, the excess interaction of hydrazine hydrate was assumed to be prevented. Cu nanoparticles are distributed homogeneously in PVA nanofibers, which showed that wormlike micelle structure could be preserved during electrospinning. The SEM micrograph of the nanofibers is shown in Figure 4.16.

This was the most successful result of the experiments carried so far. The fibers with Cu nanoparticles inside could be produced at this process conditions.

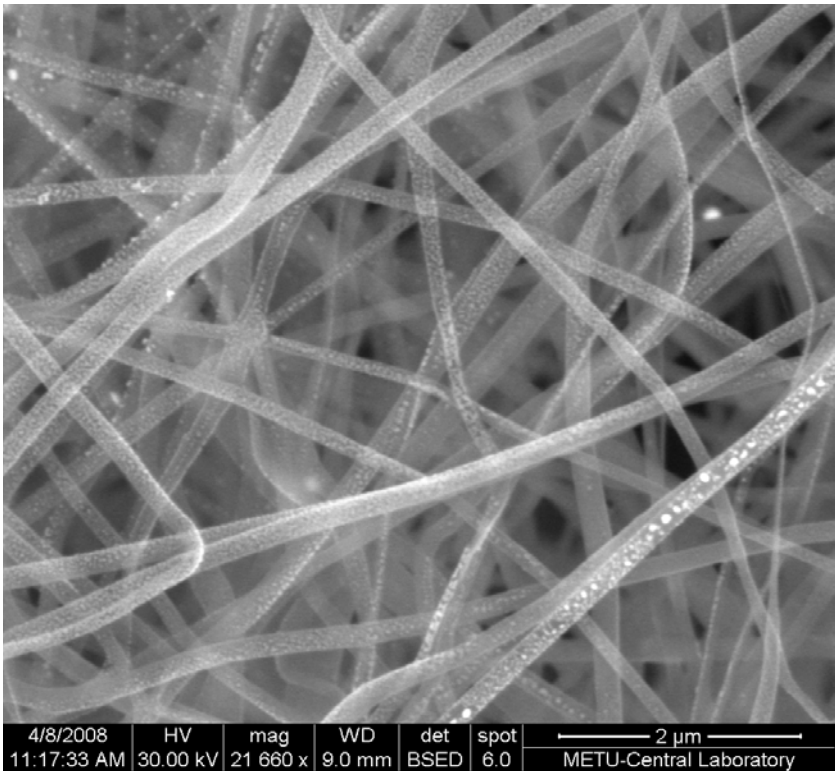

**Figure 4.16** SEM micrograph of nanofibers with a Cu to hydrazine hydrate ratio of 1:2.5 (V:16 kV, d:15 cm, feedrate:0.8ml/h).

Generally, the SEM analysis of the polymer samples is done at an operating voltage of 10 kV. In order to increase the contrast between the PVA and Cu nanoparticles, the operating voltage was increased to 30 kV. The Cu nanoparticles in the upper portion of the nanofibers scattered more electrons. This could lead to an artifact where they appear larger as compared to the Cu nanoparticles below.

The elemental analysis of Cu nanoparticles was done by using Energy Dispersive X-Ray Analysis (EDX) probe of SEM. The result of EDX analysis is shown in Figure 4.17. Gold is also detected in the elemental analysis of the sample since samples were coated with a 4 nm thick gold layer to decrease the charging effects.

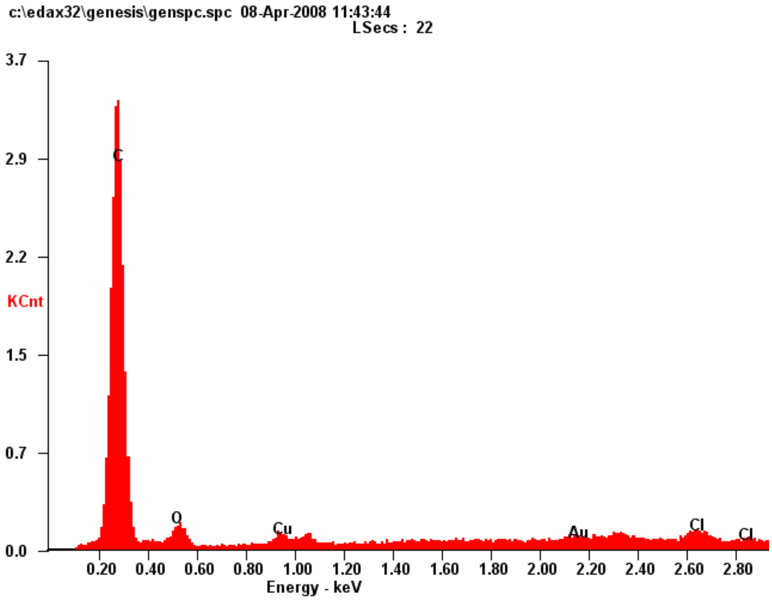

| Element | Wt % | At % |
|---|---|---|
| C K (α) | 67.30 | 85.00 |
| O K (α) | 09.48 | 08.99 |
| Cu K (α) | 14.40 | 04.38 |
| Au M (α) | 06.09 | 00.47 |

**Figure 4.17** EDX spectra and elemental analysis of the nanofibers shown in Figure 4.14.

The amount of hydrazine hydrate was further decreased to investigate its effect on the morphology of the nanofibers. It was found that for a Cu/hydrazine hydrate ratio of 1:2 the reduction reaction was not completed, and only a few Cu nanoparticles were appeared in the polymer matrix. The SEM picture is shown in Figure 4.18.

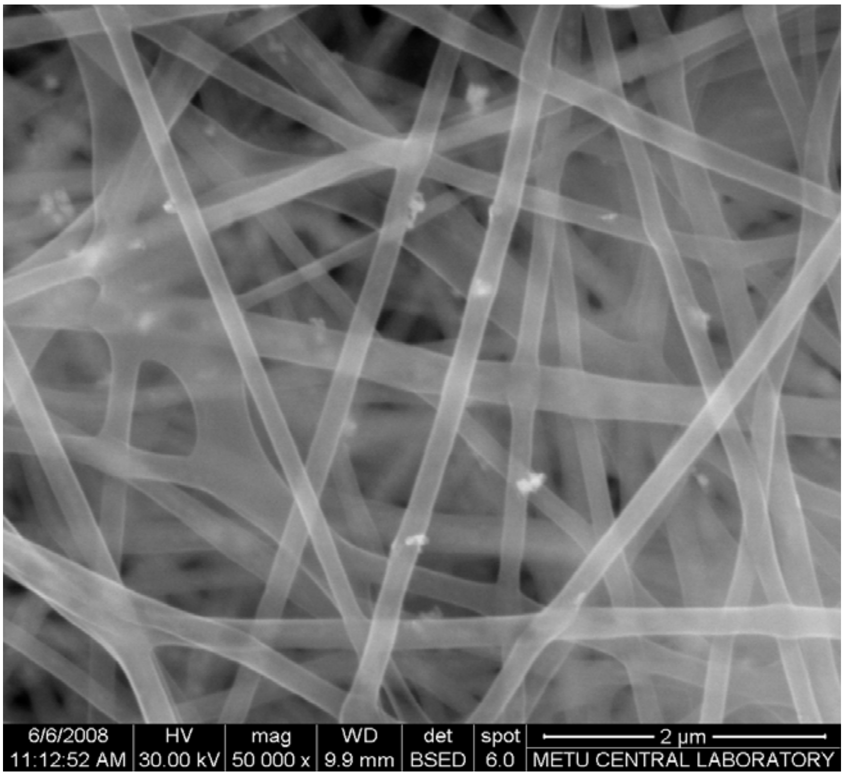

**Figure 4.18** SEM micrograph of nanofibers with copper to hydrazine hydrate ratio 1:2 (V:16 kV, d:15 cm, feedrate:0.8ml/h).

## 4.4 Diameter Measurements of the Nanofibers

SEM images have been used and processed using ImageJ (Image Processing and Analysis in Java) to measure the diameter of electrospun nanofibers. Average size of nanofibers was found to be between 125 and 150 nm. The diameters of the nanofibers with their standard deviation are shown in Table 4.4 for the samples having different copper to hydrazine hydrate ratio.

As the homogeneity of nano particles was achieved the variation in size of fibers decreased. The raw data of size analyses was given in Appendix B.

**Table 4.4** Size analysis of electrospun nanofibers.

| $n_{Cu}/n_{HYD.}$ | **Average Size of Nanofibers (nm)** | **Size of Copper Nanoparticles (nm)** |
|---|---|---|
| 1:2.5 | 144.0±24 | 20.0±3 |
| 1:3.5 | 138.1±26 | 72.7±6 |
| 1:5 | 137.1±60 | 248.6±23 |

As shown in Table 4.4, average nanofiber diameter is affected from the molar ratio of Cu to hydrazine hydrate. The average particle size of nanofibers did not vary much.

# CHAPTER 5

# CONCLUSIONS

1. The desired 1-D metal/polymer composite structure was successfully obtained through a 3 step route;
    i. Reversed wormlike micelle formation,
    ii. Reduction of metal ions within the micelles,
    iii. Electrospinning of the solution.

2. Effects of polymer and surfactant concentration on the reversed micelle formation were identified. It was seen that average particle size of wormlike micelles increases with the polymer and surfactant concentration. However, increasing polymer and surfactant concentration beyond a certain level causes extreme gelation of the solution. At this point, the micelles are agglomerated instead of staying isolated and individual.

3. The maximum micelle size measurable by DLS with proper opacity and viscosity is achieved for a solution having 12% PVA and $2.25\times10^{-3}$ M DSS. Further increase in concentration did not reveal reliable measurements.

4. Prompt addition of hydrazine hydrate to the solution resulted in the reduction only in the portions of the solution readily in contact with hydrazine hydrate. If the amount of hydrazine hydrate is increased to

complete the reduction, molecules close to the surface are exposed to excessive hydrazine hydrate. This results in the destruction of wormlike micelles and deteriotion of the desired nanofiber structures. Therefore, hydrazine hydrate addition rate is decreased and the optimum addition rate is determined to be 0.25 ml/min.

5. The optimum amount of hydrazine hydrate to avoid bridging effect on Cu and PVA is also investigated. The optimum ratio of Cu ions to hydrazine hydrate is found to be 1:2.5 which leads to the homogenous distribution of Cu nanoparticles in PVA nanofibers.

6. The relation between wormlike micelle size and the distribution of Cu in PVA was investigated. The optimum wormlike micelle size determined to be between 420 – 450 nm to distribute Cu nanoparticles homogeneously in PVA. In case of larger micelle sizes, Cu particles observed to leave the micelle structure, and they are observed on the surface of the nanofibers.

7. Temperature and electric field application on reversed wormlike micelle structure is found to adversely affect the nanofiber morphology. Temperature was applied to increase the mobility of surfactant molecules and enhance the wormlike micelle formation. However, this caused the enlargement of the micelles beyond the optimum sizes as described in the previous item. The electric field was applied to regulate the arrangement of micelles in the solution, however, coagulation of copper ions was observed as the result of the application of electric field. This was also observed in the SEM micrographs.

8. Proper electrospinning conditions were identified for beadless and continuous nanofiber formation. It was found that for a solution having 8% PVA, feed rate should be set to 0.8 ml/h, and 16 kV DC voltage should be applied.

# CHAPTER 6

# RECOMMENDATIONS

Further development of this work could be the formation of core – shell structured nanofibers through coaxial electrospinning technique. The solution prepared in this study can be used as core fluid and a proper polymer solution can be selected as the shell fluid. By coaxial spinning of the solution, nanocable structures can be formed.

Oleil amine can be used as a reduction agent instead of hydrazine hydrate to lead slower reduction reaction of metal ions in the solution. This may lead to a more efficient control of the structure of reversed wormlike micelles due to the weak reduction strength of oleil amine as compared to hydrazine hydrate.

# REFERENCES

1. Huang Z. M., Zhang Y. Z., Kotaki M., and Ramakrishna S., A review on polymer nanofibers by electrospinning and their applications in nanocomposites. *Composites Science and Technology* **2003,** 63, (15), 2223-2253.

2. Huang Z. M., Zhang Y. Z., Ramakrishna S., and Lim C. T., Electrospinning and mechanical characterization of gelatin nanofibers. *Polymer* **2004,** 45, (15), 5361-5368.

3. Yang F., Murugan R., Wang S., and Ramakrishna S., Electrospinning of nano/micro scale poly(L-lactic acid) aligned fibers and their potential in neural tissue engineering. *Biomaterials* **2005,** 26, (15), 2603-2610.

4. Kim I. D., Rothschild A., Lee B. H., Kim D. Y., Jo S. M., and Tuller H. L., Ultrasensitive Chemiresistors Based on Electrospun TiO2 Nanofibers. *Nano Letters* **2006,** 6, (9), 2009-2013.

5. Yang Q. B., Li D. M., Hong Y. L., Li Z. Y., Wang C., Qiu S. L., and Wei Y., Preparation and Characterization of a PAN Nanofibre Containing Ag Nanoparticles via Electrospinning. *Synthetic Metals* **2003,** 137, (1-3), 973-974.

6. Khanna P. K., Singh N., Charan S., Subbarao V. S., Gokhale R., and Mulik U. P., Synthesis and characterization of Ag/PVA nanocomposite by chemical reduction method. *Materials Chemistry and Physics* **2005,** 93, (1), 117-121.

7. Sadjadi M. A., Sadeghi B., Meskinfam M., Zare K., and Azizian J., Synthesis and characterization of Ag/PVA nanorods by chemical reduction method. *Physica E: Low-dimensional Systems and Nanostructures* **2008,** 40, (10), 3183-3186.

8. Songping W., Preparation of ultra fine nickel-copper bimetallic powder for BME-MLCC. *Microelectronics Journal* **2007,** 38, (1), 41-46.

9. Li Z., Huang H., and Wang C., Electrostatic Forces Induce Poly(vinyl alcohol)-Protected Copper Nanoparticles to Form Copper/Poly(vinyl alcohol) Nanocables via Electrospinning. *Macromolecular Rapid Communications* **2006,** 27, (2), 152-155.

10. Xi L. F. and Lam Y. M., Synthesis and characterization of CdSe nanorods using a novel microemulsion method at moderate temperature. *Journal of Colloid and Interface Science* **2007,** 316, (2), 771-778.

11. Chen W., Li C. M., Chen P., and Sun C., Electrosynthesis and characterization of polypyrrole/Au nanocomposite. *Electrochimica Acta* **2007,** 52, (8), 2845-2849.

12. O'Shaughnessy B. and Yu J., Rheology of Wormlike Micelles:Two Universality Classes. *Physical Review Letters* **1995,** 74, (21), 4329-4332.

13. Huibers D. T., Lobanov V. S., Katritzky A. R., Shah D. O., and Karelson M., Prediction of Critical Micelle Concentration Using a Quantitative Structure-Property Relationship Approach. *Journal of Colloid and Interface Science* **1997,** 187, (1), 113-120.

14. Acharya D. P., Kunieda H., Shiba, Y., and Aratani K., Phase and Rheological Behavior of Novel Gemini-Type Surfactant Systems. *The Journal of Physical Chemistry B* **2004,** 108, (5), 1790-1797.

15. Rosen J. M., *Surfactants and Interfacial Phenomena*. John Wiley & Sons Incorporated: 2004.

16. Wang D., Song. C., Fu X., and Hu Z., Surfactant-Assisted Synthesis of Cube-Shaped PbTe and PbSe Nanocrystals. *Journal of Dispersion Science and Technology* **2007,** 28, (8), 1197-1200.

17. Liu Y., Cao J., Li C., Zeng J., Tang K., Qian Y., and Zhang W., Hydrazine route to one-dimensional structural metal selenides crystals. *Journal of Crystal Growth* **2004,** 261, (4), 508-513.

18. Du J., Xu L., Zou G., Chai L., and Qian Y., A solvothermal method to novel metastable ZnSe nanoflakes. *Materials Chemistry and Physics* **2007,** 103, (2-3), 441-445.

19. Ghosh D. and Dasgupta S., Synthesis of Submicron Silver Powder by the Hydrometallurgical Reduction of Silver Nitrate with Hydrazine Hydrate and a Thermodynamic Analysis of the System. *Mettalurgical and Materials Transactions B* **2008,** 39 B, 35-45.

20. Charlton I. D. and Doherty A. P., Electrochemistry in true reverse micelles. *Electrochemistry Communications* **1999,** 1, (5), 176-179.

21. Wu H., Xu, J., He X., Zhao Y., and Wen H., Mesoscopic simulation of self-assembly in surfactant oligomers by dissipative particle dynamics. *Colloids and Surfaces A: Physicochemical and Engineering Aspects* **2006,** 290, (1-3), 239-246.

22. Wulfsberg G., *Inorganic Chemistry*. University Science Books: 2000.

23. Tansel B., Sager J., Rector T., Garland J., Strayer R. F., Levine L., Roberts M., Hummerick M., and Bauer, J., Significance of hydrated radius and hydration shells on ionic permeability during nanofiltration in dead end and cross flow modes. *Separation and Purification Technology* **2006,** 51, (1), 40-47.

24. Hait S. K. and Moulik S. P., Gemini surfactants: A distinct class of self-assembling molecules. *Current Science* **2002,** 82, (9), 1101-1111.

25. Faeder J. and Ladanyi B. M., Molecular Dynamics Simulations of the Interior of Aqueous Reverse Micelles. *The Journal of Physical Chemistry B* **2000,** 104, (5), 1033-1046.

26. Mohammad A. and Hena S., Use of sodium bis (2-ethyl hexyl) sulfosuccinate (AOT) anionic surfactant mobile phase systems in thin-layer chromatography of amino acids: simultaneous separation of thioamino acids. *Chromatography* **2004,** 24, (5), 111-118.

27. Cringus D., Bakulin A., Lindner J., Vohringer P., Pshenichnikov M. S., and Wiersma D. A., Ultrafast Energy Transfer in Water&#x2212;AOT Reverse Micelles. *The Journal of Physical Chemistry B* **2007,** 111, (51), 14193-14207.

28. Sato T. and Einaga Y. Dynamic Light Scattering from Non-Entangled Wormlike Micellar Solutions.

29. Yadong Li and Wang Y. D. Z., A Novel Chemical Route to ZnTe Semiconductor Nanorods. *Advanced Materials* **1999,** 11, (10), 847-850.

30. Demir M. M., Gökçe U., Gülgün M. A., and Menceloğlu Y. Z., Glycidyl-Methacrylate-Based Electrospun Mats and Catalytic Silver Nanoparticles. *Macromolecular Chemistry and Physics* **2008,** 209, (5), 508-515.

31. Lo H., Kadiyala S., Guggino S.E., and Leong K.W., Poly(L-lactic acid) foams with cell seeding and controlled-release capacity. *Journal of Biomedical Materials Research* **1996,** 30, (4), 475-484.

32. Ma X. P. and Zhang R., Synthetic nano-scale fibrous extracellular matrix. *Journal of Biomedical Materials Research* **1999,** 46, (1), 60-72.

33. Frenot A. and Chronakis I. S., Polymer nanofibers assembled by electrospinning. *Current Opinion in Colloid & Interface Science* **2003,** 8, (1), 64-75.

34. Hartgerink J. D., Beniash E., and Stupp S. I., Self-Assembly and Mineralization of Peptide-Amphiphile Nanofibers. *Science* **2001,** 294, (5547), 1684-1688.

35. Harfenist S. A., Cambron S. D., Nelson E. W., Berry S. M., Isham A. W., Crain M. M., Walsh K. M., Keynton R. S., and Cohn R. W., Direct Drawing of Suspended Filamentary Micro- and Nanostructures from Liquid Polymers. *Nano Letters* **2004,** 4, (10), 1931-1937.

36. Joachim T. and Ondarcuhu C., Drawing a single nanofibre over hundreds of microns. *EPL (Europhysics Letters)* **1998,** 42, (2), 215.

37. Christopherson G. T., Song H., and Mao H. Q., The influence of fiber diameter of electrospun substrates on neural stem cell differentiation and proliferation. *Biomaterials* **2009,** 30, (4), 556-564.

38. Kenawy E. R., Abdel-Hay F. I., El-Newehy M. H., and Wnek G. E., Processing of polymer nanofibers through electrospinning as drug delivery systems. *Materials Chemistry and Physics* **2009,** 113, (1), 296-302.

39. Zhang L. and Webster T. J., Nanotechnology and nanomaterials: Promises for improved tissue regeneration. *Nano Today* **2009,** 4, (1), 66-80.

40. Formhals A., Process and apparatus for preparing artificial threads., 54, 1934.

41. Taylor G. I., Electrically Driven Jets. *Proc. of Roy. Soc. of London* **1969,** 313, 453-475.

42. Chen M., Zhou J., Xie L., Gu G., and Wu L., Facile Fabrication Method of PS/Ni Nanocomposite Spheres and Their Catalytic Property. *J. Phys. Chem. C* **2007,** 111, (32), 11829-11835.

43. Subbiah T., Tock R. W., Parameswaran S., and Ramkumar J. S., Electrospinning of Nanofibers. *Journal of Applied Polymer Science* **2005,** 96, 557-569.

44. Keun Son W., Ho Youk J., Seung Lee T., and Park W. H., Effect of pH on electrospinning of poly(vinyl alcohol). *Materials Letters* **2005,** 59, (12), 1571-1575.

45. Chuangchote S., Fabrication of Aligned Poly(vinyl alcohol) Nanofibers by Electrospinning. *Journal of Nanoscience and Nanotechnology* **2006,** 6, 125-129.

46. Wen Ji J., Lee K. H., Jeong H. E., Park W. H., and Youk J. H., Preparation of Polymer Nanofibers Containing Silver Nanoparticles by Using

Poly(vinylpyrrolidone). *Macromolecular Rapid Communications* **2005,** 26, (24), 1903-1907.

47. Hyeyoung Kong J. J., One-step fabrication of silver nanoparticle embedded polymer nanofibers by radical-mediated dispersion polymerization. *Chemical communications* **2006,** 1, 3010-3012.

48. Hamlett C. A., Jayasinghe S. N., and Preece J. A., Electrospinning nanosuspensions loaded with passivated Au nanoparticles. *Tetrahedron* **2008,** 64, (36), 8476-8483.

49. Asano T., Levrenz H. L., Tsuchihashi R., and Tchobanoglous G., *Water Reuse:Issues, Technologies and Applications*. Mc Graw Hill Proffessional: 2007.

50. *Handbook of Chemistry and Physics*. Chemical Rubber Company: Ohio, 1972-1973.

# APPENDIX A

# RAW DATA OF DYNAMIC LIGHT SCATTERING MEASUREMENTS

**Table A.1** Effect of Changing PVA and DSS Amount on Average Particle Size.

| DSS (g) | Average Diameter (nm) | Peak Width (nm) |
|---|---|---|
| **4% PVA** | | |
| 0,001 | 14,99 | 7,137 |
| 0,001 | 14,45 | 1,831 |
| 0,001 | 14,3 | 7,307 |
| 0,005 | 19,85 | 6,868 |
| 0,005 | 20,3 | 2,92 |
| 0,005 | 18,1 | 2,477 |
| | | |
| **6% PVA** | | |
| 0,001 | 16,01 | 8,727 |
| 0,001 | 18,6 | 9,897 |
| 0,001 | 19,23 | 2,419 |
| 0,005 | 21,13 | 2,751 |
| 0,005 | 20,32 | 2,581 |
| 0,005 | 21,44 | 2,729 |
| 0,01 | 23,57 | 3,155 |
| 0,01 | 26,81 | 3,637 |
| 0,01 | 22,7 | 2,89 |
| | | |
| **8% PVA** | | |
| 0,001 | 197,7 | 74,99 |
| 0,001 | 207,1 | 72,58 |
| 0,001 | 192,6 | 69,37 |
| 0,005 | 222,6 | 83,31 |

**Table A.1** Effect of Changing PVA and DSS Amount on Average Particle Size (continued).

| | | |
|---|---|---|
| 0,005 | 210,7 | 63,36 |
| 0,005 | 212,9 | 69,66 |
| 0,01 | 238,6 | 86,72 |
| 0,01 | 233,1 | 81,13 |
| 0,01 | 233,1 | 81,13 |
| 0,02 | 256,6 | 73,24 |
| 0,02 | 269,5 | 89,66 |
| 0,02 | 260,8 | 100,9 |
| | | |
| **10% PVA** | | |
| 0,001 | 274,8 | 120,9 |
| 0,001 | 267,5 | 78,99 |
| 0,001 | 269,8 | 78,54 |
| 0,005 | 289,2 | 112 |
| 0,005 | 298,1 | 132,9 |
| 0,005 | 283,8 | 106,5 |
| 0,01 | 310,6 | 123,6 |
| 0,01 | 316,6 | 119,4 |
| 0,01 | 310,9 | 98,83 |
| 0,02 | 344,1 | 119,7 |
| 0,02 | 341,6 | 96 |
| 0,02 | 334 | 95,3 |
| 0,03 | 451,9 | 151,3 |
| 0,03 | 432,7 | 135,2 |
| 0,03 | 450,4 | 127 |
| **12% PVA** | | |
| 0,001 | 340,4 | 134,7 |
| 0,001 | 346,5 | 144,7 |
| 0,001 | 329,2 | 95,78 |
| 0,005 | 375,6 | 131,2 |
| 0,005 | 352,5 | 132,6 |
| 0,005 | 373,4 | 135,9 |
| 0,01 | 405,3 | 112,1 |
| 0,01 | 420,4 | 112,4 |
| 0,01 | 410,9 | 130,2 |
| 0,02 | 428,1 | 143,7 |
| 0,02 | 428,6 | 151,6 |
| 0,02 | 448,4 | 156,1 |

**Table A.2** Effect of Heating, Electric Field and Application Time of the Electric Field on Average Particle Size.

| Applied Voltage | Average Diameter | Peak Width |
|---|---|---|
| **t:4h, T:25$^0$C** | | |
| 0 | 430,4 | 125,6 |
| 0 | 453,3 | 132,5 |
| 0 | 424,9 | 130,7 |
| 5000 | 538,7 | 122,8 |
| 5000 | 578,8 | 131,9 |
| 5000 | 527,2 | 126,3 |
| 7000 | 648,9 | 162,7 |
| 7000 | 650 | 159,8 |
| 7000 | 634,7 | 157,3 |
| | | |
| **t: 1h, T:25$^0$C** | | |
| 0 | 435,5 | 123,8 |
| 0 | 438 | 121,9 |
| 0 | 437 | 121,2 |
| 1000 | 455,3 | 124,1 |
| 1000 | 448,4 | 120,9 |
| 1000 | 451,9 | 118 |
| 3000 | 462,5 | 126,1 |
| 3000 | 465,6 | 112,9 |
| 3000 | 468,7 | 124,3 |
| 5000 | 531,5 | 143,5 |
| 5000 | 489,9 | 123,3 |
| 5000 | 533,6 | 187,5 |
| | | |
| **t:1h, T:40$^0$C** | | |
| 0 | 454,3 | 126,4 |
| 0 | 452,9 | 151,7 |
| 0 | 426,7 | 139,1 |
| 1000 | 478,1 | 156,7 |
| 1000 | 480,9 | 142,8 |
| 1000 | 488,2 | 144 |
| 3000 | 520,2 | 150,7 |
| 3000 | 491,6 | 132 |

**Table A.2** Effect of Heating, Electric Field and Application Time of the Electric Field on Average Particle Size (continued).

| | | |
|---|---|---|
| 3000 | 518 | 146,3 |
| 5000 | 552,9 | 152,5 |
| 5000 | 585,8 | 170,1 |
| 5000 | 551,7 | 147,2 |
| | | |
| **t:1h, T:60$^0$C** | | |
| 0 | 481,5 | 96,28 |
| 0 | 533,8 | 116,4 |
| 0 | 486,5 | 121,5 |
| 1000 | 675,5 | 133,2 |
| 1000 | 833 | 154,8 |
| 1000 | 626 | 132,4 |
| 2000 | 721,2 | 139,2 |
| 2000 | 746,9 | 145,7 |
| 2000 | 772,8 | 125,5 |
| 3000 | 700,7 | 150,4 |
| 3000 | 724 | 112,5 |
| 3000 | 755,8 | 141 |
| 4000 | 570,1 | 105,5 |
| 4000 | 770,6 | 141,9 |
| 4000 | 586,4 | 134,3 |
| 5000 | 531,7 | 97,29 |
| 5000 | 534,1 | 115,5 |
| 5000 | 520,7 | 101,7 |

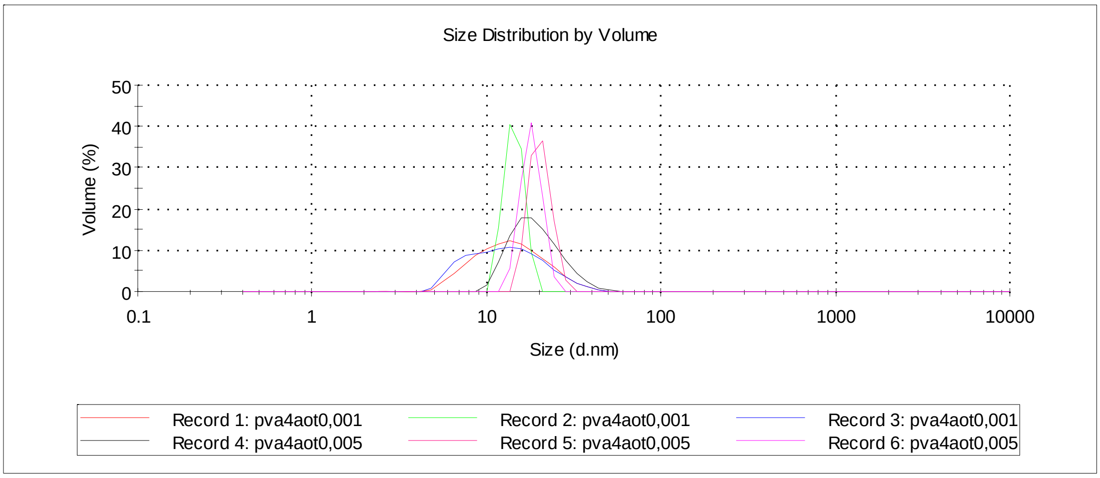

**Figure A.3** Average particle size distribution with 4% PVA solution.

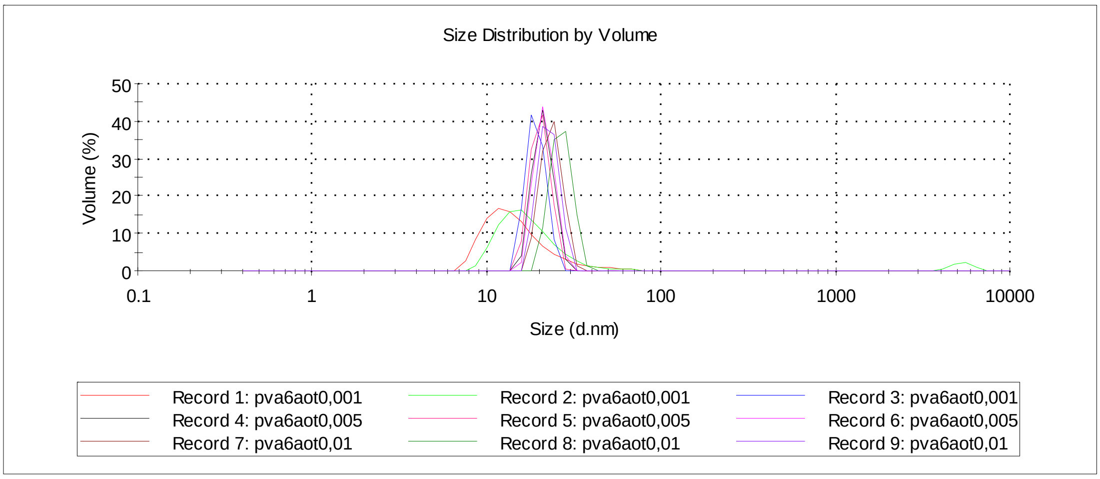

**Figure A.4** Average particle size distribution with 6% PVA solution.

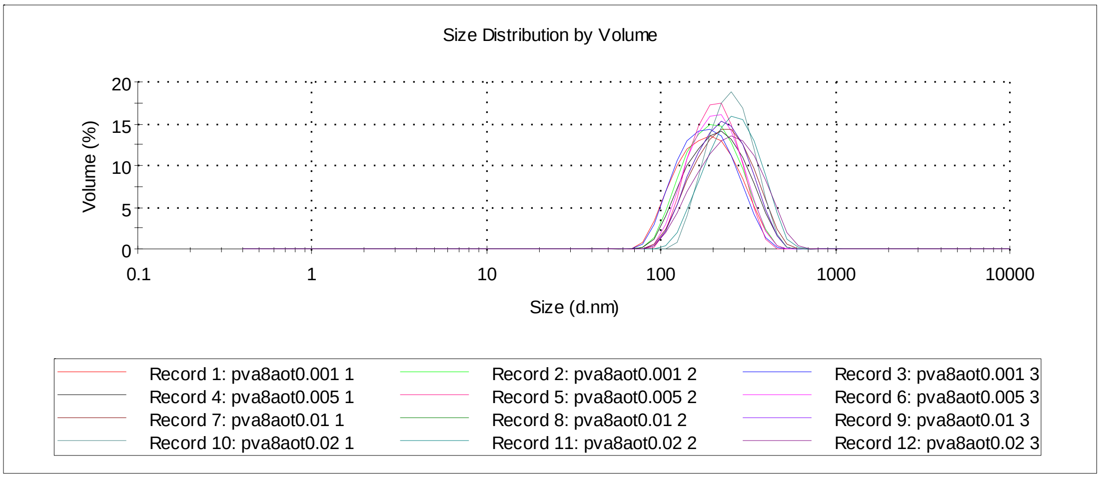

**Figure A.5** Average particle size distribution with 8% PVA solution.

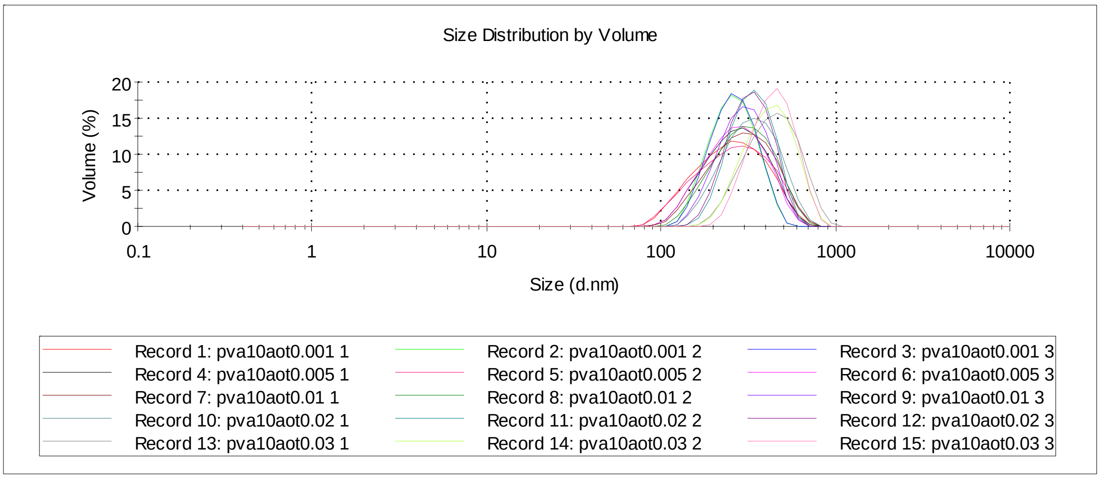

**Figure A.6** Average particle size distribution with 10% PVA solution.

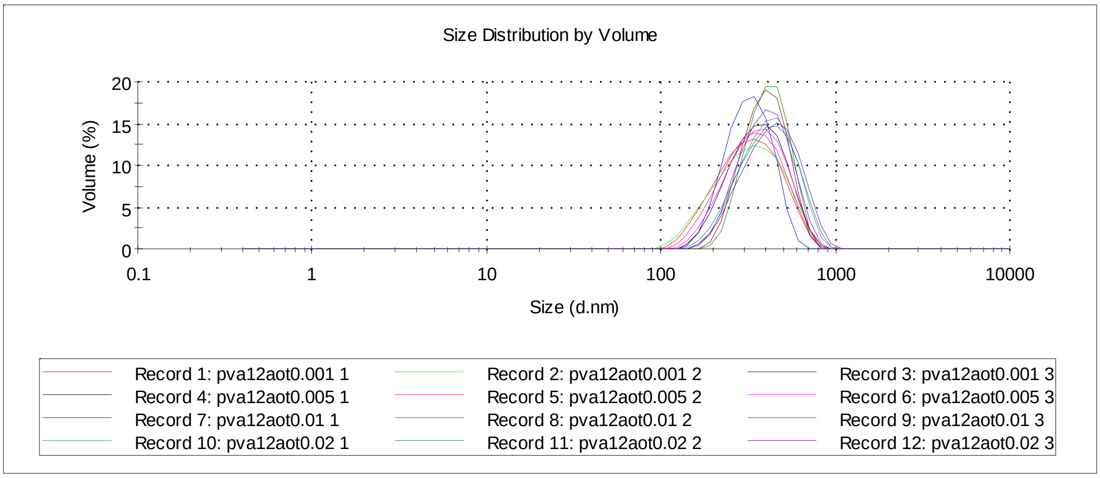

**Figure A.7** Average particle size distribution with 12% PVA solution.

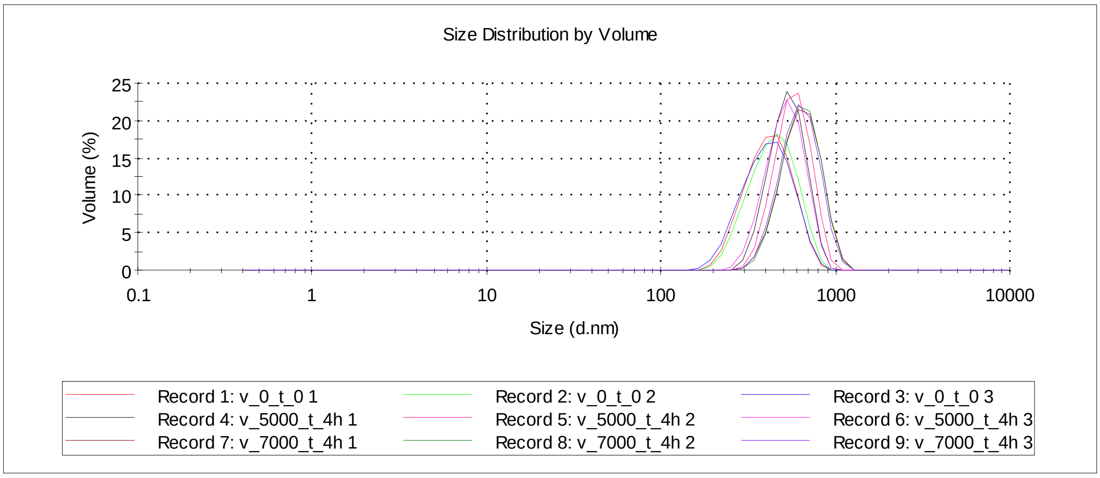

**Figure A.8** Effect of electric field on average particle size at $25^0$C with 4h application time.

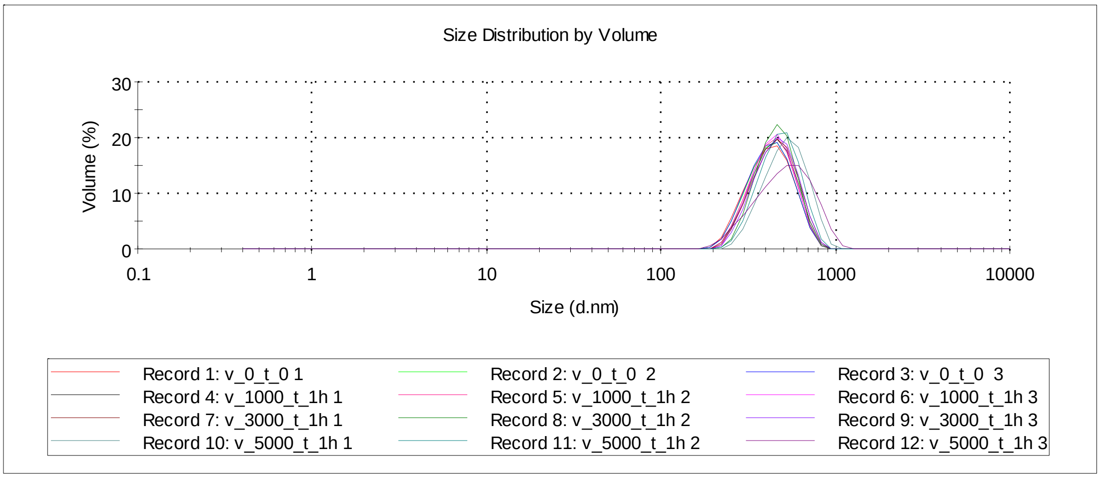

**Figure A.9** Effect of electric field on average particle size at 25$^0$C with 1h application time.

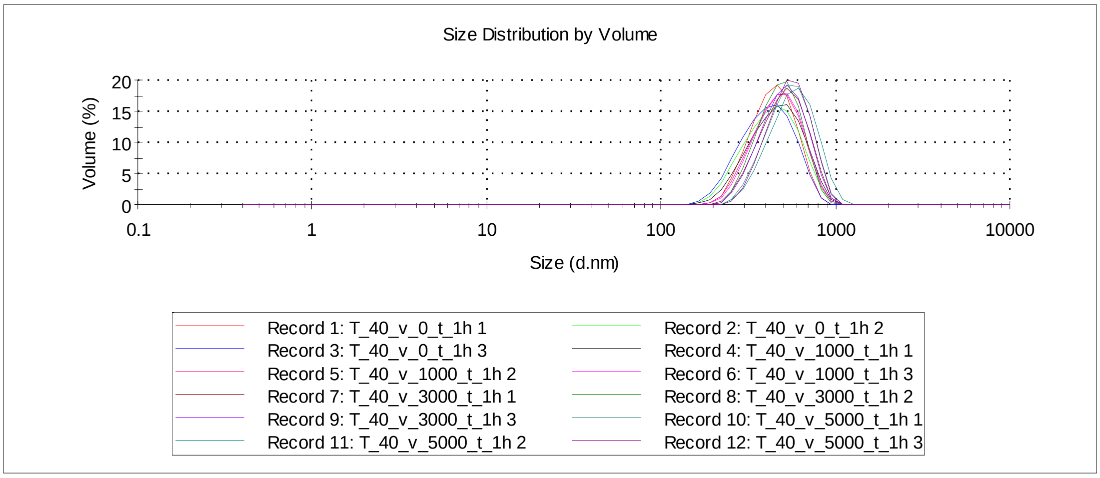

**Figure A.10** Effect of electric field on average particle size at 40$^0$C with 1h application time.

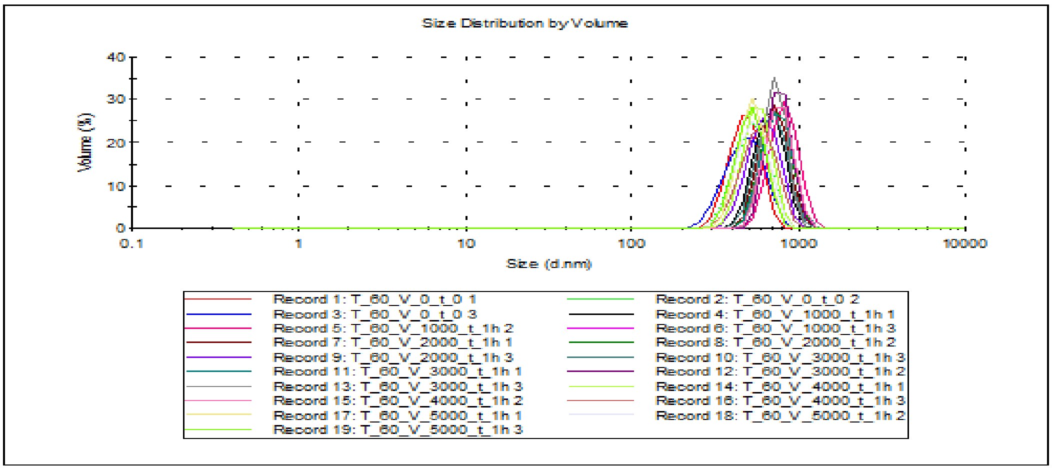

**Figure A.11** Effect of electric field on average particle size at $60^0$C with 1h application time.

# APPENDIX B

# RAW DATA OF FIBER SIZE MEASUREMENTS

**Table B.1** Size measurements of the sample having hydrazine hydrate to copper ratio 2.5.

| | Mean | Minimum | Maximum | Angle | Length |
|---|---|---|---|---|---|
| 1 | 188.212 | 173.206 | 220.787 | -28.443 | 185.901 |
| 2 | 176.487 | 121.752 | 208.341 | -50.194 | 157.814 |
| 3 | 161.926 | 154.810 | 168.514 | -90 | 136.153 |
| 4 | 128.290 | 106.640 | 157.541 | -108.435 | 149.630 |
| 5 | 132.936 | 114.814 | 146.614 | -158.199 | 141.153 |
| 6 | 147.845 | 130.694 | 171.564 | 19.440 | 122.452 |
| 7 | 128.083 | 106.351 | 145.749 | 14.036 | 111.246 |
| 8 | 158.419 | 140.468 | 174.437 | -115.201 | 125.148 |
| 9 | 153.812 | 141.038 | 184.993 | -53.130 | 169.123 |
| 10 | 132.520 | 120.622 | 143.297 | -81.254 | 173.322 |
| 11 | 167.813 | 151.492 | 210.811 | -57.724 | 151.166 |
| 12 | 161.850 | 114.506 | 199.560 | -36.469 | 194.936 |
| 13 | 153.245 | 147.525 | 159.245 | -128.660 | 91.769 |
| 14 | 154.002 | 140.438 | 164.824 | -138.576 | 152.351 |
| 15 | 107.850 | 99.315 | 116.083 | -80.538 | 123.704 |
| 16 | 138.199 | 111.542 | 158.872 | -38.047 | 193.614 |
| 17 | 130.209 | 112.964 | 146.335 | -140.528 | 147.730 |
| 18 | 125.494 | 118.081 | 133.612 | -78.111 | 132.134 |
| 19 | 132.398 | 125.544 | 140.076 | -78.111 | 132.134 |
| 20 | 128.807 | 112.628 | 159.311 | -145.008 | 164.973 |
| 21 | 104.887 | 100.842 | 109.591 | 45 | 116.654 |
| 22 | 138.969 | 122.577 | 149.221 | 26.565 | 153.860 |
| 23 | 130.736 | 122.607 | 138.061 | -58.241 | 167.138 |

**Table B.1** Size measurements of the sample having hydrazine hydrate to copper ratio 2.5.(continued)

| | | | | | |
|---|---|---|---|---|---|
| 24 | 143.351 | 138.087 | 151.888 | -51.340 | 127.587 |
| 25 | 119.442 | 109.487 | 124.304 | -130.236 | 117.531 |
| 26 | 154.807 | 125.284 | 185.670 | -40.601 | 188.098 |
| 27 | 176.506 | 153.520 | 211.344 | -77.471 | 125.148 |
| 28 | 139.351 | 128.366 | 153.394 | -45 | 111.476 |
| 29 | 135.755 | 111.832 | 156.287 | 8.130 | 144.923 |
| 30 | 120.987 | 112.475 | 126.563 | -47.490 | 111.476 |

**Table B.2** Size measurements of the copper nano particles in sample having hydrazine hydrate to copper ratio 2.5.

| | Mean | Minimum | Maximum | Angle | Length |
|---|---|---|---|---|---|
| 1 | 185.256 | 149.002 | 219.837 | -33.690 | 25.391 |
| 2 | 197.887 | 196.708 | 199.795 | -45 | 9.959 |
| 3 | 160.570 | 155.345 | 164.458 | -26.565 | 15.747 |
| 4 | 214.497 | 211.503 | 216.499 | -63.435 | 15.747 |
| 5 | 174.932 | 148.863 | 188.160 | -63.435 | 31.494 |
| 6 | 177.111 | 173.381 | 185.457 | -18.435 | 22.270 |
| 7 | 157.155 | 144.213 | 166.312 | -90 | 14.085 |
| 8 | 134.970 | 130.049 | 138.508 | 0 | 14.085 |
| 9 | 138.763 | 124.810 | 148.444 | -14.036 | 29.036 |
| 10 | 173.673 | 170.613 | 177.207 | 18.435 | 22.270 |

**Table B.3** Size measurements of the sample having hydrazine hydrate to copper ratio 3.5.

| | Mean | Minimum | Maximum | Angle | Length |
|---|---|---|---|---|---|
| 1 | 166.783 | 136.333 | 202.667 | -119.358 | 124.040 |
| 2 | 149.592 | 125.333 | 165.333 | 33.024 | 160.962 |
| 3 | 117.783 | 105.333 | 132.227 | 48.814 | 139.469 |
| 4 | 85.787 | 67.667 | 91.689 | 21.801 | 144.245 |
| 5 | 122.564 | 115.347 | 126.853 | -53.973 | 89.286 |
| 6 | 175.957 | 143.667 | 198.769 | 8.973 | 262.749 |
| 7 | 159.046 | 95.667 | 182.333 | -48.814 | 145.347 |
| 8 | 167.011 | 131 | 189.800 | -108.435 | 132.733 |
| 9 | 158.651 | 141.667 | 177.578 | -149.036 | 156.186 |
| 10 | 113.027 | 100.778 | 121.949 | -71.565 | 149.670 |
| 11 | 147.909 | 124 | 165.006 | -51.340 | 126.899 |
| 12 | 157.466 | 135.889 | 176.185 | 28.811 | 151.786 |
| 13 | 129.182 | 121.667 | 135.565 | -33.690 | 148.601 |
| 14 | 155.688 | 114 | 169.627 | -90 | 169.643 |
| 15 | 113.764 | 108.333 | 119.884 | 17.103 | 93.217 |
| 16 | 98.197 | 74 | 112.333 | 11.310 | 136.581 |
| 17 | 148.280 | 114 | 175.372 | -110.854 | 152.571 |
| 18 | 103.436 | 94.893 | 117 | 48.013 | 88.388 |
| 19 | 125.349 | 121.294 | 132.726 | -92.490 | 152.048 |
| 20 | 143.550 | 140.333 | 146.581 | 29.055 | 71.984 |
| 21 | 114.644 | 109.667 | 119.293 | 17.103 | 93.217 |
| 22 | 123.417 | 95.667 | 132.481 | 3.013 | 125.318 |
| 23 | 116.132 | 87.333 | 130.250 | 7.125 | 107.514 |
| 24 | 101.415 | 96.309 | 105.815 | -102.529 | 119.122 |
| 25 | 108.602 | 93.333 | 115.167 | 4.764 | 160.962 |
| 26 | 86.749 | 79.111 | 89.841 | 0 | 151.786 |
| 27 | 52.433 | 36.667 | 58.211 | -41.424 | 152.048 |
| 28 | 141.586 | 127.333 | 150.654 | 22.380 | 124.361 |
| 29 | 96.093 | 74.111 | 106.889 | -45 | 189.404 |
| 30 | 87.660 | 71 | 97.224 | 14.744 | 130.002 |

**Table B.4** Size measurements of the copper nano particles in sample having hydrazine hydrate to copper ratio 3.5.

| | Mean | Minimum | Maximum | Angle | Length |
|---|---|---|---|---|---|
| 1 | 218.825 | 135.333 | 255 | -18.435 | 151.700 |
| 2 | 227.483 | 154.667 | 255 | -28.072 | 113.392 |
| 3 | 252.859 | 237.667 | 255 | -32.471 | 85.375 |
| 4 | 217.361 | 186.778 | 233.098 | -55.008 | 77.848 |
| 5 | 233.020 | 185.667 | 249.222 | -90 | 63.348 |
| 6 | 220.507 | 192 | 237 | 0 | 63.348 |
| 7 | 220.252 | 171 | 251.427 | -75.069 | 103.182 |
| 8 | 211.101 | 167.333 | 234.733 | -36.870 | 70.680 |
| 9 | 236.749 | 189 | 255 | -55.008 | 85.375 |
| 10 | 224.854 | 172.444 | 251.526 | -90 | 99.546 |

**Table B.5** Size measurements of the sample having hydrazine hydrate to copper ratio 5.

| | Mean | Minimum | Maximum | Angle | Length |
|---|---|---|---|---|---|
| 1 | 235.040 | 162.333 | 255 | -90 | 161.433 |
| 2 | 123.278 | 116.333 | 135 | -39.806 | 107.995 |
| 3 | 214.274 | 195.969 | 248 | -49.764 | 114.853 |
| 4 | 166.581 | 102 | 223.667 | 26.565 | 148.455 |
| 5 | 107.230 | 97.750 | 115.222 | -19.654 | 104.974 |
| 6 | 34.758 | 0 | 53.333 | -13.392 | 147.913 |
| 7 | 240.756 | 217.333 | 255 | 19.093 | 181.599 |
| 8 | 131.963 | 125.077 | 148.667 | -83.991 | 125.879 |
| 9 | 159.320 | 141.556 | 181.040 | 17.819 | 198.527 |
| 10 | 208.970 | 193.335 | 231.057 | -57.724 | 149.266 |
| 11 | 147.256 | 135.012 | 167.071 | -77.471 | 128.410 |
| 12 | 90.602 | 60.778 | 112.328 | -30.964 | 156.885 |
| 13 | 102.358 | 72.444 | 118.907 | 3.013 | 125.879 |
| 14 | 131.053 | 122.931 | 143.486 | 32.735 | 116.935 |
| 15 | 57.020 | 47.067 | 64.347 | 22.834 | 136.604 |
| 16 | 62.697 | 50.625 | 83 | -57.265 | 109.475 |
| 17 | 122.299 | 106.852 | 153.222 | -46.736 | 158.669 |
| 18 | 76.573 | 59.333 | 83.367 | 23.629 | 116.591 |
| 19 | 201.317 | 187.667 | 219.190 | 15.945 | 150.340 |
| 20 | 197.643 | 157 | 217.776 | 16.390 | 121.985 |
| 21 | 169.530 | 150.333 | 183.392 | -75.964 | 139.229 |
| 22 | 131.058 | 108.667 | 149.533 | -67.166 | 136.604 |
| 23 | 40.152 | 19 | 61.436 | -90 | 89.685 |
| 24 | 86.789 | 55.889 | 99.222 | -104.036 | 110.934 |
| 25 | 113.854 | 85 | 126.911 | 5.711 | 134.826 |
| 26 | 41.821 | 2.333 | 64.687 | -79.992 | 117.962 |
| 27 | 73.949 | 54 | 83.123 | -116.565 | 120.325 |
| 28 | 94.284 | 27 | 114.044 | -23.962 | 136.604 |
| 29 | 54.099 | 19.962 | 115.369 | -82.569 | 153.516 |
| 30 | 77.923 | 65.222 | 84.082 | 24.775 | 96.594 |

**Tablo B.6** Size measurements of the copper nano particles in sample having hydrazine hydrate to copper ratio 3.5.

| | Mean | Maximum | Minimum | Angle | Length |
|---|---|---|---|---|---|
| 1 | 245.248 | 190 | 255 | -87.709 | 164.020 |
| 2 | 239.543 | 195.396 | 255 | -125.074 | 370.790 |
| 3 | 252.191 | 224.067 | 255 | -45.659 | 792.541 |